Geochemical evidence of mantle reservoir evolution during progressive rifting along the western Afar margin

Tyrone O. Rooney, Paul J. Mohr, Laure Dosso, Chris Hall

Available online at www.sciencedirect.com

SciVerse ScienceDirect

Geochimica et Cosmochimica Acta 102 (2013) 65–88

Geochimica et Cosmochimica Acta

www.elsevier.com/locate/gca

Geochemical evidence of mantle reservoir evolution during progressive rifting along the western Afar margin

Tyrone O. Rooney [a,*], Paul Mohr [b], Laure Dosso [c], Chris Hall [d]

[a] Dept. of Geological Sciences, Michigan State University, East Lansing, MI 48824, USA
[b] Tonagharraun, Corrandulla, Co. Galway, Ireland
[c] Laboratoire Domaines Océaniques, UMR 6538, CNRS, Ifremer, 29280 – Plouzané, France
[d] Dept. of Earth and Environmental Sciences, University of Michigan, Ann Arbor, MI 48109, USA

Received 21 February 2011; accepted in revised form 20 August 2012; available online 26 August 2012

Abstract

The Afar triple junction, where the Red Sea, Gulf of Aden and African Rift System extension zones converge, is a pivotal domain for the study of continental-to-oceanic rift evolution. The western margin of Afar forms the southernmost sector of the western margin of the Red Sea rift where that margin enters the Ethiopian flood basalt province. Tectonism and volcanism at the triple junction had commenced by ~31 Ma with crustal fissuring, diking and voluminous eruption of the Ethiopian-Yemen flood basalt pile. The dikes which fed the Oligocene-Quaternary lava sequence covering the western Afar rift margin provide an opportunity to probe the geochemical reservoirs associated with the evolution of a still active continental margin. $^{40}Ar/^{39}Ar$ geochronology reveals that the western Afar margin dikes span the entire history of rift evolution from the initial Oligocene flood basalt event to the development of focused zones of intrusion in rift marginal basins. Major element, trace element and isotopic (Sr-Nd-Pb-Hf) data demonstrate temporal geochemical heterogeneities resulting from variable contributions from the Afar plume, depleted asthenospheric mantle, and African lithosphere. The various dikes erupted between 31 Ma and 22 Ma all share isotopic signatures attesting to a contribution from the Afar plume, indicating this initial period in the evolution of the Afar margin was one of magma-assisted weakening of the lithosphere. From 22 Ma to 12 Ma, however, diffuse diking during continued evolution of the rift margin facilitated ascent of magmas in which depleted mantle and lithospheric sources predominated, though contributions from the Afar plume persisted. After 10 Ma, magmatic intrusion migrated eastwards towards the Afar rift floor, with an increasing fraction of the magmas derived from depleted mantle with less of a lithospheric signature. The dikes of the western Afar margin reveal that magma generation processes during the evolution of this continental rift margin are increasingly dominated by shallow decompressional melting of the ambient asthenosphere, the composition of which may in part be controlled by preferential channeling of plume material along the developing neo-oceanic axes of extension.

1. INTRODUCTION

Early quantitative tectonic models explained the generation of mantle melt in extensional zones in terms of simple adiabatic decompression of the asthenosphere (e.g., White and McKenzie, 1989). However, the stresses required to rupture typical continental lithosphere may not be available from plate tectonic processes alone, and hybrid models were subsequently developed in which magma provides additional impetus for lithospheric rifting (e.g., Buck, 2004; Buck, 2006; Bialas et al., 2010). Lateral variations in lithospheric thickness and rheology may also localize strain and magmatism during rifting (e.g., Ebinger and Sleep, 1998; van Wijk et al., 2008). Upwelling, buoyant asthenosphere contributes to plate driving forces, and may generate significant volumes of melt across a broad re-

* Corresponding author. Tel.: +1 517 432 5522.
E-mail address: rooneyt@msu.edu (T.O. Rooney).

0016-7037/$ - see front matter © 2012 Elsevier Ltd. All rights reserved.
http://dx.doi.org/10.1016/j.gca.2012.08.019

gion (e.g., Huismans et al., 2001). The presence of buoyant melt can facilitate the intrusion of dikes into thick continental lithosphere at comparatively small extensional stresses, and this heating can significantly reduce the strength of the plate, further facilitating extension (e.g., Fialko and Rubin, 1999; Buck, 2004; Bialas et al., 2010). Thus, the initial phase of rifting above a mantle plume may be marked by a pulse of widespread dike intrusion (e.g., Renne et al., 1996; Fialko and Rubin, 1999; Klausen and Larsen, 2002). During the later stages of continental rifting, extension occurs principally by dike intrusion into a thinned lithosphere (Ebinger and Casey, 2001; Keranen et al., 2004; Rooney et al., 2005; Daly et al., 2008; Keir et al., 2009; Bastow et al., 2010; Ebinger et al., 2010; Wright et al., 2012), before a final stage of plate stretching and associated decompression melting characterizing the final stages of continent-ocean transition (e.g., Bastow and Keir, 2011). Key unresolved questions remain concerning the geochemical signature(s) of the melt sources during the initial stages of continental rifting, and the evolution of these sources as rifting continues.

The mafic lavas and dikes of continental rift margins provide a window on the evolution of the underlying mantle sources that have contributed to a developing rift. Unfortunately, most rifted margins are now at least partly submarine and relatively inaccessible. However, sustained uplift above an active mantle plume in Ethiopia has provided a sub-aerial instance of a continental rift margin in the final stages of its evolution. Observations around the Afar triple-rift junction confirm that magmatic intrusion and crustal heating have played a significant role in facilitating lithospheric extension and rupture (Berckhemer et al., 1975; Mohr, 1983a; Buck, 2004; Buck, 2006; Bialas et al., 2010; Bastow and Keir, 2011). The western margin of Afar provides an excellent site for probing the space–time relationships between magmatism and extension across a rift margin (e.g., Keir et al., 2011b). In this paper we examine the geochemical, structural, and geochronological properties of the dikes that intrude this continental margin, and explore the participation of the various mantle and lithospheric geochemical reservoirs that contribute to the evolution of this margin.

2. THE WESTERN AFAR RIFT MARGIN

2.1. Setting and form

The well-studied western Afar margin separates the stable and relatively undeformed post-basement cover of the Ethiopian Plateau to the west from the Cenozoic and presently active extensional faulting, fissuring, and magmatism of the Afar depression (Gortani and Bianchi, 1937; Abbate et al., 1968; Abbate and Sagri, 1969; Mohr, 1971; Megrue et al., 1972; Gortani and Bianchi, 1973; Justin-Visentin and Zanettin, 1974; Mohr, 1983a; Hart et al., 1989; Wolfenden et al., 2005). The 800-km long western Afar margin runs in a gently curvilinear plan from Asmara in the north to Addis Ababa in the south, with the exception of a large dextral offset at latitude 13°N (Fig. 1). This coincides with the northern limit of the thick flood-lava sequence on the plateau, and also marks a structural contrast: to the north, seismically active stepped normal faults downthrown towards the rift are concentrated within a narrower margin (40 km); to the south, antithetically faulted flood-basalts cap a wider (80 km) monoclinal margin (Mohr, 1962; Abbate and Sagri, 1969; Ayele et al., 2007; Keir et al., 2011a). This southern sector of the margin can in turn be divided into two sub-sectors to either side of a proposed accommodation zone (Wolfenden et al., 2005). North of latitude 11°N, the flood-basalt pile comprises 31–29 Ma lavas and tuffs locally overlain by a cover of ~25–22 Ma flows (Justin-Visentin and Zanettin, 1974; Kieffer et al., 2004). Proceeding south from 11°N to Addis Ababa, the Oligocene flood-basalt pile is capped by progressively younger lavas that include a volumetrically significant proportion of silicic members (Zanettin, 1992; Ukstins et al., 2002). The margin transect chosen for this study is located immediately north of the chronological divide at 11°N (Fig. 1), taking advantage of the Desse-Eloa highway (Mohr, 1971; Gortani and Bianchi, 1973).

2.2. Regional stratigraphy

Expanding upon earlier studies detailing the stratigraphic and structural characteristics of the western Afar margin (Abbate et al., 1968; Gortani and Bianchi, 1973; Justin-Visentin and Zanettin, 1974; Mohr, 1983b), a new stratigraphy for the entire southern sector of the western Afar margin has been compiled by Wolfenden et al. (2005). It comprises four magmatic episodes (Table 1) which relate to a sequential, riftward production of three elongate rift-parallel volcanic basins imposed on the regional Oligocene flood-basalt pile:

The ‘Stage 1 Basin’ developed at the western end of the transect, contemporaneous with eruption of basalts and agglomerates derived from the 25–22 Ma-old Guguftu shield volcano located on the plateau rim (Kieffer et al., 2004). These Dese Formation lava flows are rarely more than a few meters thick, and lie with local unconformity on the lateritized and strongly zeolitised Oligocene pile. Characteristic lithologies are megacrystic plagioclase basalt, aphyric basalt, and subordinate olivine- and olivine-augite-phyric basalt. The pyroclastic members include fine basaltic tuff (in one instance carrying blocks of underlying, unexposed Jurassic limestone) and massive agglomerate proximate to basalt pipe vents. Silicic ash-fall and ash-flow tuff beds are restricted to the topmost part of the Dese Formation. The ‘Stage 2 Basin’ is situated near the median of the Desse-Eloa transect. Its fill of flood basalts and intercalated ignimbrites compose the early-mid Miocene Burka Formation (Wolfenden et al., 2005), again lying with unconformity on the Oligocene stratoid pile. The ‘Stage 3 Basin’ at the eastern end of the transect contains the late Miocene-Pliocene Dahla Series basalts, previously termed Fursa Basalts (Justin-Visentin and Zanettin, 1974).

2.3. Dikes and faults of the Desse–Eloa transect

Antithetic faulting parallel to the NNW regional strike of the margin has produced tilted crustal blocks typically

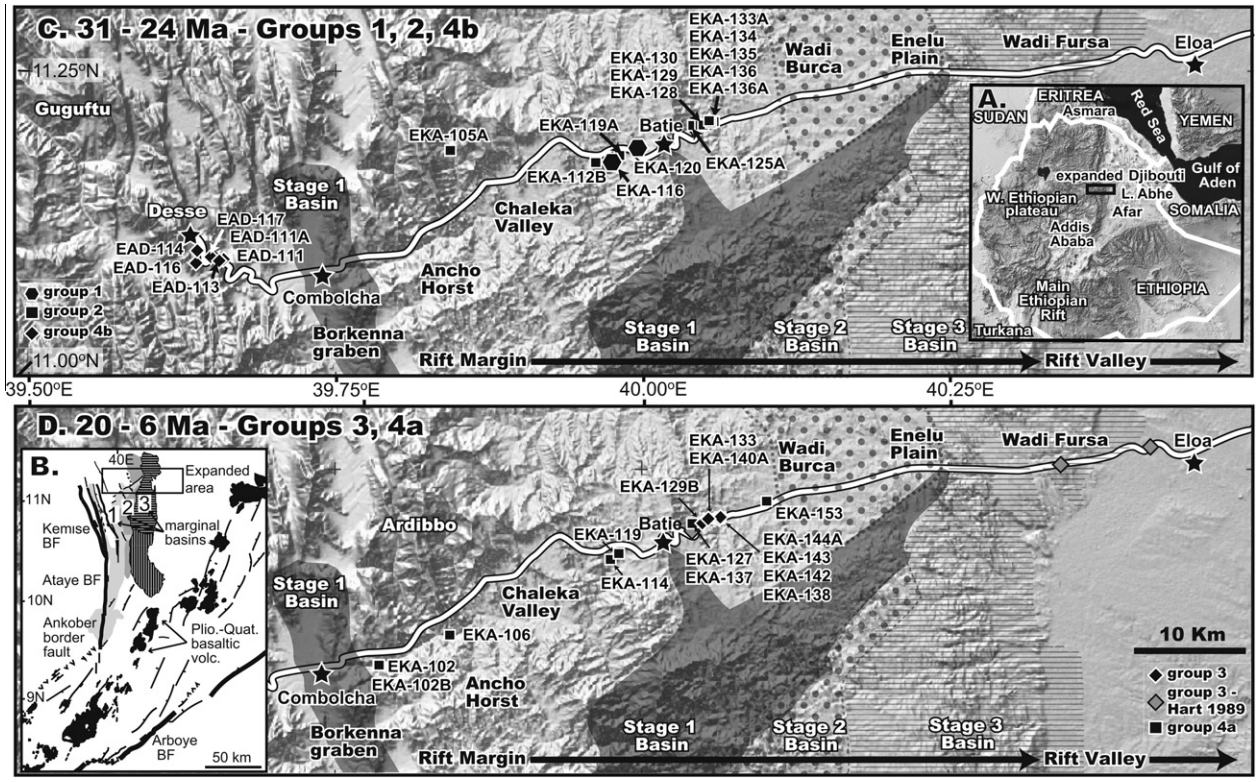

Fig. 1. Spatial distribution of dike samples throughout the region. The approximate alignment of the Desse–Eloa highway is shown for reference. Topography is a digital elevation model based on the NASA/JPL SRTM dataset. The structural basins outlined by Wolfenden et al. (2005) are outlined: stage 1 basin – dark grey filling, stage 2 basin – dotted fill, stage 3 basin – vertical lines. Additional samples presented in Hart et al. (1989) are also shown. Towns referred to in the text are denoted by stars. (A) Inset region is topography of the Afar triple junction region showing the broad structural features including the Main Ethiopian Rift, Red Sea, and Gulf of Aden; (B) Inset of the regional tectonic framework focusing on structural basins (labeled 1–3; Wolfenden et al., 2005). Pliocene-Quaternary basaltic magmatism within the Ethiopian rift is also shown for reference (Rooney et al., 2011); (C) Dikes from ~20 to 6 Ma (Groups 3, 4a); (D) Dikes from 31–24 Ma (Groups 1, 2, 4b).

Table 1
Summary of the existing stratigraphic groups defined by Wolfenden et al. (2005).

Unit	Composition	Basin	Age	Dike group
Dahla series	Fissure Basalts	3	c. 7–5 Ma*	3
Unconformity				
Burka formation	Basalts, rhyolites	2	c. 20–13 Ma	4a
Unconformity				
Dese Formation	Basalts	1	c. 29.5–24 Ma	1,4b
Unconformity				
Ashangi, Aiba, Alaji	Flood basalts, rhyolites	Throughout	c. 31.5–29.5**	2

* Renne et al., 1996.
** Hofmann et al., 1997.

10–20 km across (Abbate and Sagri, 1969; Mohr, 1983b). The resultant dips of the Oligocene stratoid pile average 20–30° in the west sector of the transect, 15°-30° in the central sector, and 15–20° in the east (Table 2). However, occasional deep gorge exposures reveal maximum dips of 30° in the west and 45° in the east, indicative of second-generation block faulting (Morton and Black, 1975). Fault-plane dip is directed overwhelmingly westward, and averages 80° in the western sector. Common 70° dips in the central and eastern sectors are interspersed with local 35°-45° dips. The predominating margin-parallel faults can number up to forty within a kilometer-wide zone, the largest with measured throws in excess of one hundred meters, the majority with west-side downthrows. Subordinate faults oblique to the regional trend include N-dipping ENE faults (yielding a southerly component of dip to the stratoid pile), S-dipping WNW faults, and W-dipping NNE faults (Mohr, 1971). Striations on some fault planes prove a component of lateral slip. Small sinusoidal folds with ENE-trending axes are pervasive in some areas.

Nearly 80 percent of all dikes strike parallel or near-parallel to the dominant NNW-trending faults that define the

Table 2
Summary of dike and fault trends across the Afar margin between Desse and Eloa, presented in detail elsewhere (Mohr, 1971).

Sector	Dikes		Faults	
	Strike	Dip	Strike	Dip
Desse-Combolcia				
	N000–010°	W	N350–000°	W, E
	N060°	Near-vertical	N065–080°*	NW
Combolcia-Batie				
	N330–350°	W	N335–350°	W, E
	N020–030°	W	N020–040°	NW
	N045–060°	NW,SE	N040–075°	NW
	N300°	SW		
Batie-Eloa				
	N330–350°	W	N340–350°	**
	N000–010°	W	N005–030°	W
	N050–060°	Near-vertical	N060–080°	NW

* This fault trend coincides with the axes of numerous small, gentle folds in the stratoid lavas.
** The NNW-trending faults of the Batie-Eloa sector dip predominantly W (with E upthrows), but in the easternmost, Eloa zone the slip planes dip E.

margin. The oblique strikes of a minority of dikes are mirrored by subordinate fault trends (Table 2). However, while dikes and faults share common conjugate trends within the western Afar margin (Abbate and Sagri, 1969; Mohr, 1971; Justin-Visentin and Zanettin, 1974; Mohr, 1983b), the major zones of fissuring and fracturing are separate and rarely overlap. The tendency to spatial segregation of fault zones and dike swarms in the western Afar margin may owe not only to temporal separation of the two processes in an evolving stress field, but also to the role, as yet not fully evaluated, of magmatic centers from which dikes were laterally propagated. The longest *exposed* dike identified in the transect is almost one kilometer, but a consideration of dikes elsewhere in Ethiopia makes it likely that some may extend for at least 10 km (Mohr, 1999; Schultz et al., 2008). The median dike width over the entire Desse-Eloa transect is 1.5 m, with a mean of 3.5 m (Mohr, 1971, 1983b).

Dike distribution across the Desse-Eloa transect is irregular (Mohr, 1971, Fig. 1), in part influenced by local volcanic centers to north and south. At the western plateau end of the transect, between Desse (2525 m) and Combolcha (1875 m), a pattern of Oligo-Miocene antithetic faulting trending N-NNW (now largely masked under Miocene Guguftu volcanics) has been superposed with complex Quaternary marginal graben faulting (Mohr, 1962). Near Dessie, Oligo-Miocene fault-blocks are tilted 10–30° (rarely as steeply as 45°) directed between E and NE, whereas near Combolcia tilts of 20–30° are directed between E and SE. The dikes exposed in this sector relate almost wholly to the covering Guguftu volcanic sequence, and trend N–S, slightly oblique to the NNW-SSE regional structural trend. Dike dips range between 60° and vertical, directed west as for the major faults (Mohr, 1971; Mohr, 1983b). Subordinate dikes trending ENE persist further eastward into the central sector of the transect.

The descent east from Combolcha and the Ancharo rim of the Borkenna graben (Fig. 1) reaches a NNW–SSE zone of intense faulting in the Chaleka valley (1520 m) (Abbate and Sagri, 1969). Through this sector of the traverse, riftward-tilted blocks of lateritized, zeolitized Oligocene flood-basalts locally manifest small sinusoidal folds also found in the Desse–Combolcia sector. Feeder dikes for the lavas are mostly in 3-D parallelism with the regional NNW-trending faults, and strike towards the Ardibbo volcanic center, 40 km to the north. Large (<35 m-wide) feeder pipes also occur, ringed with precursor, intensely baked agglomerate. Subordinate dikes of ESE trend (SW dip) and NNE trend (W dip) can form a symmetrical complementary pair about the dominant NNW dikes. If synchronous, they indicate a maximum principal horizontal stress directed along the strike of the margin (Mohr, 1971), concurring with the geometry of the folds and some small reversed faults in the flood-basalt pile.

From the Chaleka valley east up to the Batie saddle (1670 m), interspersed NNW and NNE-trending dikes expose no cross-cutting relationships. Some NNW dikes became normal slip planes during solidification, but others were subject to later oblique, brittle displacement. For example, intrusion EKA-119, a 6 m-wide, near-vertical N300° dike was displaced by a N030° fault dipping 75° SE, the 3-D orientation of neighboring NNE dikes.

Down the eastern slope of the Batie saddle, the transect declines rapidly to Wadi Burca (1000 m), then more gently onto the Enelu plain (950 m). From the eastern side of the plain (Wadi Fursa), the decline resumes to Eloa (675 m) at the western edge of the Afar floor (Fig. 1). Between 4 and 8 km east of Batie, both dikes and faults are numerous and share a NNE trend distinctly oblique to the regional margin trend. The maximum measured dilatation for the entire Desse-Eloa transect occurs here: a total dike width of 60 m opened within a 1 km-wide crustal strip, indicating 6% extension. East from this swarm for 15 km, limited exposures of tilted Oligocene flood-basalts in the Burca valley ('Stage 2 Basin' of Wolfenden et al., 2005) reveal rare

thin, fractured dikes, until more typical dikes resume in the Fursa valley ('Stage 3 Basin' of Wolfenden et al., 2005).

3. ANALYTICAL TECHNIQUES

Dikes in preference to lavas have been selected for this study, as they form in response to both the structural and magmatic evolution of the margin. Furthermore, flood basalt lavas can flow significant distances from their vents, thus potentially skewing spatial studies.

3.1. Geochronology

Ten representative samples that did not exhibit any indications of alteration were selected for $^{40}Ar/^{39}Ar$ step heating analysis at the Argon Geochronology Laboratory at the University of Michigan. Fresh matrix chips (0.2 g) were carefully handpicked under a binocular microscope and Ar analysis was undertaken using standard procedures outlined in Frey et al. (2007). Samples were wrapped in pure Al foil packets and irradiated in location 5C of the McMaster Nuclear Reactor. Samples were step-heated using a continuous 5 W Ar-ion laser and Ar isotopes were analyzed using a VG-1200S mass spectrometer operating with a total electron emission setting of 150 micro-amps (see Table 3 and Supplemental table for further analytical information).

3.2. Major and trace elements

Thirty-five samples (1–2 kg) were taken from the least-altered dikes, and for each dike from a position intermediate between the center and margin. They were subsequently trimmed to exclude visible alteration/weathering. Sample billets were polished to remove saw marks and cleaned in an ultra sonic bath with deionised water. After drying, the billets were crushed in a steel jaw-crusher and then powdered in a ceramic Bico flat plate grinder. The sample powders were fused into lithium tetraborate glass disks using the procedures outlined in Deering et al. (2008). Major elements, Zr, Sr, Rb and Ni were analyzed by Brucker XRF, the balance of the trace elements were obtained by laser-ablation using a Cetac LSX-200 coupled to a Micromass Platform ICP-MS at Michigan State University. Trace element reproducibility based on standard analyses (see Supplemental Data) is typically better than 5% (Vogel et al., 2006).

3.3. Isotope Geochemistry

Twelve representative samples of the western Afar dikes were chosen for radiogenic isotope analysis at the Laboratoire Domaines Océaniques of CNRS/Ifremer, France. Samples were chosen on the basis of a) representing all dike groups, and b) selecting the most primitive magmas possible. Powdered samples (300–600 mg) were dissolved in Savillex beakers using ultrapure concentrated HF-HBr (3:1 in volume). Separation and analyses of Pb, Hf, Sr and Nd were performed from the same sample dissolution using 4 different columns.

Column 1: to minimize Pb blanks, Pb separation was performed first, using the standard anion exchange method in an HBr medium (Tilton, 1973; Manhes et al., 1978). After loading the sample, the Pb column was washed with 0.5 M HBr. The fraction passing through the column directly following loading and subsequent washing was collected and evaporated in 6 M HCl for further separation of Hf-Sr-Nd on column 2. We repeated the anion exchange method a second time to purify the Pb fraction which was collected in 6 M HCl.

Column 2 : the Hf-Sr-Nd fraction was taken up in 0.5 M HCl/0.15 M HF and loaded on a cation column (microcolumn Savillex, 30 ml, 6.4 mm ID × 9.6 mm OD × 25 cm). The Hf-Ti fraction was eluted in the first 6 ml with 0.5 M HCl/0.15 M HF. 22 ml of 3 M HCl was then added to the column to wash for Fe and Rb, and the Sr fraction was then collected in 6 ml and evaporated to dryness. 8 ml of 4 M HNO_3 was then added to the same column to separate Ba from the rare earth elements, which were then recovered in a 6 ml fraction.

Column 3: following evaporation, the rare earth fraction was placed on a Biorad Econo-Col Polyprop 0.8 × 4 cm loaded with Eichrom LN resin. Nd was separated from Ce and Sm using 13 ml of 0.2 M HCl and eluted using 4 ml of 0.35 M HCl.

Column 4: the Hf-Ti fraction separated using column 2 is evaporated and taken up in 6 M HCl containing a trace of H_2O_2. The Hf-Ti separation was performed using a 5 ml pipette tip loaded with 100 mg of Eichrom LN resin that was washed with 6 M HCl. 10 ml 6 M HCl with 50 µl of H_2O_2 were used to elute Ti. Hf was subsequently collected in 5 ml of 2 M HF.

Pb, Nd, and Hf were analyzed by MC-ICPMS on the Thermo Neptune at Ifremer. Sr was analyzed by TIMS using the Finnigan MAT-26X also located at Ifremer. Standards, blanks and analytical errors are given in the caption to Table 4.

4. RESULTS AND CLASSIFICATION OF DIKES

4.1. Geochronology

4.1.1. Cross-cutting relationships

Pervasive zeolitisation of the Oligocene stratoid lavas, and to a lesser extent their feeder dikes, was accomplished before intrusion of the 25–22 Ma-old Guguftu dikes, consistent with the expected thermal history of a 1 km-thick lava pile (Walker, 1960; Jepsen and Athearn, 1962). The essentially perpendicular relationship of the flood basalt lavas to the great majority of dikes indicates that ratchet faulting and block tilting of the lava pile occurred after fissuring and magmatic injection was largely accomplished. Nevertheless, in some cases the time interval between fissuring faulting was brief, as evidenced by ductile deformation along dike axes. Young intra-margin faulting is exemplified in a 12 Ma-old dike (EKA-119 on the Batie saddle) displaced by a NNE-trending fault. In general, however, field studies across the western Afar margin are not yet sufficient to distinguish the relative age-relationships among the several trends of dikes and faults.

Table 3
$^{40}Ar/^{39}Ar$ geochronology results.

Sample	Run	TGA (Ma)	+/−	RIA (Ma)	+/−	EWP (Ma)	+/−	CIA (Ma)	+/−	Preferred (Ma)	+/−	Megrue K-Ar (Ma)	+/−
EAD-111	a	24.67	0.25	24.67	0.25	24.27	0.17						
	b	23.89	0.21	23.95	0.18	23.56	0.16						
	Avg.	24.20	0.39	24.21	0.34	23.90	0.36	23.57	0.17	23.57	0.17	23.9	2.0
EAD-114	a	24.43	0.06	24.76	0.06	NA	–						
	b	24.58	0.08	24.77	0.08	NA	–						
	Avg.	24.48	0.07	24.76	0.05	–	–	24.82	0.13	24.76	0.05	23.1	0.9
EKA-112B	a	31.02	0.26	30.74	0.21	30.80	0.18						
	b	31.02	0.33	31.14	0.29	30.72	0.21						
	Avg.	31.02	0.20	30.88	0.19	30.77	0.14	30.75	0.16	30.77	0.14	NA	NA
EKA-116	a	28.56	0.34	29.85	0.21	29.79	0.19						
	b	28.94	0.41	29.36	0.37	29.14	0.28						
	c	28.65	0.30	28.87	0.24	29.79	0.22						
	Avg.	28.58	0.20	29.78	0.15	29.66	0.19	30.01	0.16	29.78	0.15	35.2	1.4
EKA-119	a	13.95	0.49	11.97	0.48	12.10	0.51						
	b	15.12	0.44	14.34	0.31	14.71	0.53						
	c	12.72	0.28	12.72	0.28	12.79	0.23						
	Avg.	13.51	0.71	13.20	0.65	12.95	0.53	12.51	0.33	12.51	0.33	15.7	1.1
EKA-120	a	27.69	0.34	27.96	0.32	NA							
	b	28.05	0.46	28.29	0.43	25.96	0.51						
	c	26.71	0.21	26.90	0.21	26.15	0.29						
	Avg.	27.13	0.39	27.37	0.41	26.10	0.26	28.02	0.27	27.37	0.41	31.8	1.4
EKA-140A	a	8.00	0.10	8.03	0.09	NA	–						
	b	8.61	0.11	8.72	0.11	9.21	0.12						
	Avg.	8.26	0.30	8.31	0.34	–	–	8.18	0.30	8.31	0.34	19.6	1.1
EKA-153	a	18.67	0.07	20.47	0.09	NA	–						
	b	19.83	0.07	20.59	0.06	NA	–						
	Avg.	19.34	0.57	20.55	0.06	–	–	21.23	0.36	20.55	0.06	NA	NA

Samples EKA-120 and EKA-119 were irradiated in package number mc23, samples EKA-111 and EKA-112B were irradiated in package mc24 and samples EAD-114, EKA-140A and EKA-153 were irradiated in package mc25. Packages mc23 and mc24 were each irradiated for 15 h (45 MWh) while package mc25 was irradiated for 2 h (6 MWh). Standard hornblende MMhb-1 was used as the fluence monitor for packages mc23 and mc24. Fish Canyon Tuff biotite split 3 (FCT-3) was used as the fluence monitor for package mc25. The K-Ar age of 520.4 Ma was used for MMhb-1 in calculating J values (Samson and Alexander, 1987) and an age of 27.99 Ma was used for FCT-3, which is a value previously calibrated against MMhb-1 (Hall and Farrell, 1995). For each sample, a total gas age (TGA) was calculated by adding up all of the gas fractions for a sample run. This age should most closely mimic what would be expected from a conventional K-Ar age. In addition to the TGA values, when possible, an error weighted plateau age (EWP) was also calculated. Plateau segments were selected based on the following criteria: (a) there are a minimum of 3 contiguous gas fractions constituting at least 50% of the ^{39}Ar released; and (b) the error weighted mean of the segment passes the null hypothesis that the calculated ages are all equal using a χ^2 test at the 95% confidence level. When multiple plateau segments were available, the one with the minimum error estimate was chosen. EWP ages include the effects of scatter about the error weighted mean age. Given that the samples analyzed were whole-rock samples with fine-grained inclusions having contrasting K-concentrations, the ~80 nm recoil distance expected for ^{39}Ar might be expected to contribute a significant amount to variations in ages within an age spectrum (Turner and Cadogan, 1974). Specifically, if K-rich phases donate ^{39}Ar into neighboring K-poor sites, then if the different minerals degas at different temperatures, one would expect anomalously high ages in the K-rich minerals and anomalously low ages in the K-poor ones. In order to account for this, while still eliminating low temperature gas fractions with apparent Ar loss due to alteration and/or diffusion, Turner et al. (1978) used the concept of a "reduced plateau" age which is calculated by totaling the gas over the fractions that would have exhibited plateaus without ^{39}Ar recoil artifacts. In order to avoid confusion with the normal terminology of error weighted plateaus, we refer to these ages as reduced integrated ages (RIA), as they are calculated by integrating the gas release over a portion of the age spectrum. A combined isochron age (CIA) was calculated by combining the gas fractions for all of a sample's replicate analyses. Scatter about the best fit line was included in the CIA error estimate. Details of the isochron fits as well as the fractions used in the EWP and RIA ages are given in the supplementary material. In the case of TGA, EWP and RIA ages, an error weighted average of the ages was calculated to provide an overall sample age estimate. The TGA, EWP, RIA and CIA model age errors all include the uncertainty in J. One of the 4 model ages was chosen as a "preferred" age and the reasons for the choice of preferred age are outlined below. Laser fusion system blanks were monitored regularly (typically every 5th sample gas fraction) and typical measured blanks at masses 36, 37, 38, 39, and 40 were about 4×10^{-14}, 4×10^{-14}, 4×10^{-15}, 4×10^{-14}, and 7×10^{-12} ccSTP respectively.

Table 4
Isotopic characteristics of dikes along the Desse-Eloa transect.

Sample	$^{87}Sr/^{86}Sr$	2σ	$^{143}Nd/^{144}Nd$	2σ	$^{206}Pb/^{204}Pb$	2σ	$^{207}Pb/^{204}Pb$	2σ	$^{208}Pb/^{204}Pb$	2σ	$^{176}Hf/^{177}Hf$	2σ
EKA-116	0.704713	9	0.512710	7	18.9293	9	15.6445	9	39.0598	26	0.282983	10
EKA-120	0.704722	8	0.512686	4	19.1851	13	15.6450	12	39.3051	35	0.282898	14
EKA-112B	0.704745	8	0.512781	6	18.2061	10	15.5638	9	38.4707	28	0.282995	13
EKA-140A	0.703647	6	0.512932	5	18.2683	12	15.5452	12	38.5000	34	0.283088	9
EKA-142	0.703449	10	0.512950	5	18.2285	10	15.5337	10	38.4161	24	0.283089	10
EKA-106	0.704443	8	0.512735	5	17.9460	8	15.5449	10	38.3195	30	0.282904	8
EKA-153	0.705482	10	0.512709	6	18.0249	11	15.5863	11	38.5694	30	0.282893	9
EKA-119	0.704333	8	0.512827	6	18.5287	10	15.5897	10	38.9792	33	0.282994	8
EAD-111	0.704514	8	0.512845	4	18.8366	12	15.6562	12	39.2479	34	0.283011	11
EAD-113	0.704286	9	0.512906	6	18.9878	9	15.6600	10	39.3444	30	0.283043	8
EAD-116	0.704101	12	0.512915	4	19.3556	10	15.6960	10	39.6695	27	0.283060	10
EAD-114	0.706728	8	0.512589	7	18.2142	8	15.6332	8	38.9070	22	0.282769	8

All Hf, Pb and Nd isotope measurements were made on a Thermo Neptune multi-collector inductively coupled plasma mass spectrometer at Ifremer. Repeat measurements of the Hf isotope standard JMC 475 during the course of the analyses yielded reproducibility of 46 ppm (2σ) on $^{176}Hf/^{177}Hf$ with a value of 0.282165. The Pb isotope data are reported relative to published values for NBS 981 in Catanzaro et al. (1968). The samples were spiked with thallium to correct for mass fractionation. Based on repeated runs of NBS 981 during the course of the analyses, the estimated external precision for Pb analyses is ±0.02%, 2σ for $^{206}Pb/^{204}Pb$ and $^{207}Pb/^{204}Pb$ and ±0.03%, 2σ for $^{208}Pb/^{204}Pb$. Repeat measurements of the Nd isotope standard JNdi-1 (Tanaka et al., 2000) yielded $^{143}Nd/^{144}Nd$ values of 0.512114 ± 12 (2σ, $n = 8$). Sr isotope measurements were performed on a multicollector Finnigan MAT26X mass spectrometer upgraded by Spectromat. Replicate analyses of NBS 987 during the analysis period gave an average value of 0.71025 ± 3 (2σ, $n = 9$). Analysis of BCR-2 gave Hf-Pb-Sr-Nd values of $^{176}Hf/^{177}Hf = 0.282861 \pm 9$, $^{206}Pb/^{204}Pb = 18.7528 \pm 6$, $^{207}Pb/^{204}Pb = 15.6203 \pm 6$, $^{208}Pb/^{204}Pb = 38.7355 \pm 19$, $^{87}Sr/^{86}Sr = 0.705007 \pm 7$, $^{143}Nd/^{144}Nd = 0.512639 \pm 4$ respectively.

4.1.2. $^{40}Ar/^{39}Ar$ dating

The results of the $^{40}Ar/^{39}Ar$ analyses are shown in Table 3. Replicate analyses were performed for each sample and a series of $^{40}Ar/^{39}Ar$ model ages were calculated. Sample EAD-111 yielded plateau ages for both of the analyses that were performed, but there were also signs of a "saddle" shape to the age spectrum, suggesting a small quantity of excess ^{40}Ar. The combined isochron age (CIA) is based on a true isochron through all 26 gas fractions with a slightly elevated initial $^{40}Ar/^{36}Ar$ ratio of 298.5 Although the CIA is not significantly different from the average of the error weighted plateau age (EWP) values, we consider the CIA to be the preferred age (23.57 Ma) for this sample, because the EWP values may be slightly biased to an erroneously high age.

For sample EAD-114, there are no EWP segments and there are definite signs of ^{40}Ar loss in the lowest temperature fractions. In addition, there is a monotonic decrease in apparent ages with increasing release temperatures, which suggests that there was internal redistribution of ^{39}Ar due to recoil. Therefore, we regard the average of the reduced integrated ages (RIA) ages to be the preferred age for this unit (24.76 Ma). In contrast, sample EKA-112B has EWP values over the entire age spectrum for both replicates. All four model ages agree within error and given that there is no sign of significant Ar loss or artifacts due to recoil, the average EWP value is our preferred age for this sample (30.77 Ma).

Three replicate analyses were performed for sample EKA-116 and the age spectra show definite signs of Ar loss in the low temperature fractions, probably due to alteration minerals. Nonetheless, all three samples had EWP segments, indicating relatively good Ar retention for the higher temperature gas fractions. However, there is a nearly monotonic decline in ages with increasing release temperatures, suggesting the possibility for recoil artifacts. Therefore, we prefer the average of RIA (29.78 Ma), which avoids the Ar-loss portions of the age spectra, but correctly accounts for the possibility of internal redistribution of ^{39}Ar from recoil.

Sample EKA-119 also had three replicate analyses and all of the runs had EWP segments. However, there are definite signs of a "saddle" shape, which suggests the possibility of excess ^{40}Ar. In order to minimize the possibility of having a bias to high ages, we prefer the CIA age through 37 gas fractions, which yields an "errorchron" with an initial $^{40}Ar/^{36}Ar$ value of 297.7 and an age that is only slightly older than the average EWP age (12.51 Ma). For sample EKA-120, only two of the three analyses yielded EWP segments and because of significant apparent age variations that correspond with changes in the Ca/K ratio, we regard the average RIA age to be the most reliable age estimate (27.37 Ma).

Sample EKA-140A exhibited rather poor reproducibility and only one of the two analyses gave an EWP segment. The age of this sample is not well constrained, but we consider that the average RIA value is the best estimate for the age of this unit (8.31 Ma). For sample EKA-153, there are signs of significant Ar loss in the low temperature gas fractions and given that there are no plateau segments, the RIA average is likely to be the best date for this sample (20.55 Ma).

Table 3 also shows K-Ar ages derived from the data in Megrue et al. (1972), with ages being updated to the decay and K composition constants in Steiger and Jäger (1977) and error estimates based upon the listed error estimates

for K and $^{40}Ar^{*}$. For samples EAD-111 and EAD-114, there is very good concordance between our Ar-Ar ages and the K-Ar ages in Megrue et al. (1972). For all of the other samples, the K-Ar ages are systematically higher than the Ar-Ar ages, although in most cases, this difference is only slightly larger than the error estimate in the K-Ar age. It is possible that the K-Ar ages are biased high because of the presence of excess Ar, a common problem with dike samples. Even though some host rock samples in Megrue et al. (1972) show ages that are greater than the dike ages, Hyodo and York (1993) showed that it is possible for an excess Ar "wave" to propagate from a dike and contaminate hosting rock. Care must be taken when interpreting K-Ar data that does not have the detail that is shown in Ar-Ar age spectra. Sample EKA-140A gives an $^{40}Ar/^{39}Ar$ age which is less than half than the K-Ar age in Megrue et al. (1972), too great an age difference to be explained by excess Ar and probably due to separate samplings from two intimate populations of dikes at this locality.

4.2. Major and trace element geochemistry

On the basis of their trace element geochemistry (see Supplemental Data Tables), the dikes of the western Afar margin at latitude 11°N can be divided into four groups.

4.2.1. Groups 1 and 2 dikes (~31–27 Ma)

Group 1 dikes (~30–27 Ma) are ankaramitic dolerites. They strike NNE and are concentrated in the eastern part of the Combolcha-Batie sector. They are chemically defined by lower REE in comparison to other groups, particularly for LREE, and low LREE/HREE ratios that lead to an overall less steep REE profile (Fig. 2). Low concentrations characterize the extended trace-element plot, with diagnostic peaks for Pb, Sr and to a lesser extent, K (Fig. 3). On the basis of geochemistry, the Ethiopian (or Western) plateau has been divided into separate high- and low-titanium (HT and LT) domains (Pik et al., 1998). While this study lies well within the HT domain, Group 1 dikes have a geochemical signature that broadly resembles that of the earliest, low-titanium (LT) Ethiopian Plateau flood basalts (Kieffer et al., 2004; Beccaluva et al., 2009). Major element variation diagrams for Group 1 dolerites and LT basalts typically overlap, though Al_2O_3 is significantly lower and TiO_2 slightly elevated in the dolerites (Fig. 4a). Likewise, primitive mantle-normalized diagrams show that Group 1 dolerites and LT basalts exhibit very similar trace element patterns, excepting dike EKA-120, an augite-hyaloankaramite with slightly higher values of Nb, Ta and Sr (Fig. 3). The more incompatible trace elements, however, are enriched in the Group 1 dolerites with respect to LT basalts of equivalent MgO content (Fig. 3).

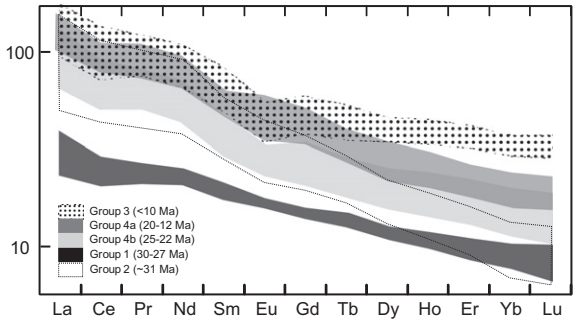

Fig. 2. Chondrite normalized (Boynton, 1984) rare earth element pattern outlining the variation among the different dike groupings. The low trace element abundance of Group 1 dikes is particularly apparent. Also of note are the low and elevated values of HREE in Groups 2 and 3 respectively.

Group 2 dikes (~31 Ma) occur spread across the Combolcha-Batie sector. These plagioclase-rich dolerites are distinguished by steep REE profiles and the highest La/Yb_{CN} (up to 11.5) of all the Afar margin dikes. Extended trace element profiles of Group 2 dolerites have features in common with Ethiopian Plateau Group 1 high-titanium flood basalts (HT-1), notably troughs for Th-U and P, and peaks for Ba and Nb-Ta (Fig. 3), consistent with the study region lying within the HT province (e.g. Pik et al., 1998). Group 2 and HT-1 samples also exhibit similar element-MgO plots (Fig. 4a), excepting elevated Sr in the dolerites that is independent of CaO (not shown). Group 2 dolerites and HT-1 basalts are distinguished from Group 2 high-titanium flood basalts (HT-2) which have more elevated TiO_2 (Fig. 4a) and more depleted HREE.

4.2.2. Group 3 dikes (<10 Ma)

Group 3 dikes are restricted to the swarm east of Batie. Group 3 and Group 1 dolerites share flat REE profiles, but the former are distinguished by higher concentrations of trace elements, excepting depletions in Sr, Eu and Ti (Fig. 3). Three basalt lava flows sampled by Hart et al. (1989) from locations between Wadi Fursa and Batie, have similar trace element characteristics to our Group 3 dolerites from the same area. Compared with Quaternary basaltic lavas from the Ethiopian rift valley (Fig. 4b), Group 3 dolerites display low Al_2O_3. They show a closer match with the major element range defined by Djibouti Holocene basaltic lavas (Deniel et al., 1994), a match which extends to trace element abundances (Fig. 4b), especially for recent Asal Rift lavas (Deniel et al., 1994), excepting that Group 3 dolerites are more enriched in HREE. The broad geochemical similarities between the Group 3 dolerites and Quaternary Afar and Ethiopian rift basalts link to their significantly younger age compared with the Groups 1 and 2 dolerites (Hart et al., 1989; this study).

4.2.3. Group 4 dikes (~25–12 Ma)

Group 4 dikes occur across the entire width of the western Afar margin at latitude 11°N. They encompass all dolerites that exhibit REE slopes intermediate between those of Groups 2 and 3 (Fig. 2). Whilst extended trace element patterns for Group 4 dolerites are broadly similar to Groups 2 and 3, REE slopes are less pronounced in comparison with Group 2 samples (Fig. 2). Matching their intermediate REE characteristics, Group 4 dolerites fall chronologically between Groups 2 and 3 (~25–12 Ma). Two subdivisions of Group 4 are identified: REE, Ti and Y abundances are higher in Group 4a dolerites compared with Group 4b (Figs. 2, 3, and 4c). Group 4a

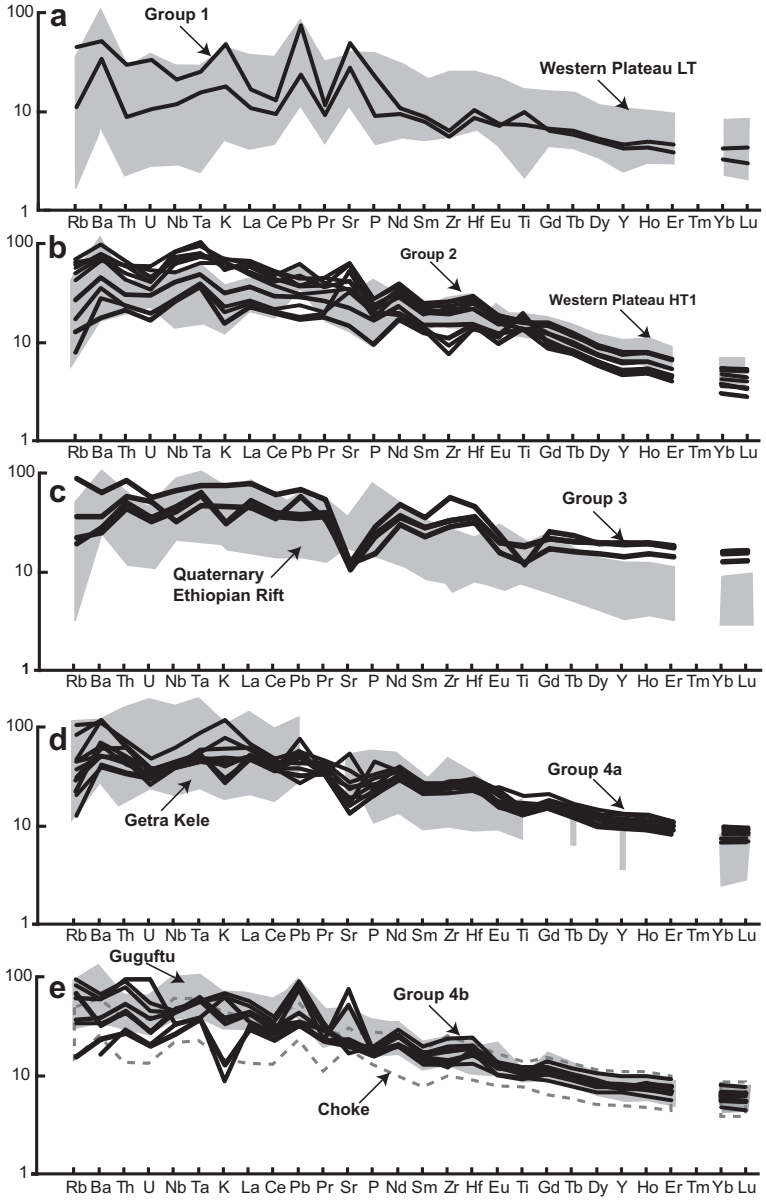

Fig. 3. Primitive mantle normalized (Sun and McDonough, 1989) trace element diagrams of dike Groups 1–4. Contemporaneous basalts are shown as shaded backgrounds for each group. (a) Low-Ti (LT) basalts from our study area (Group 1) in comparison to other LT basalts from the western Ethiopian plateau (Pik et al., 1999; Kieffer et al., 2004; Beccaluva et al., 2009). Group 1 samples plot within the range of other western plateau samples and exhibit a similar trace element pattern. (b) High-Ti type 1 (HT-1) basalts from Group 2 are plotted with HT-1 samples from the western Ethiopian plateau (Pik et al., 1999; Beccaluva et al., 2009). Patterns between both series broadly correlate though Group 2 samples extend to depleted values of the more compatible elements, and higher values of Nb-Ta in comparison to other HT-1 basalts. (c) Group 3 basalts are shown in comparison to Quaternary volcanic rocks from the Main Ethiopian Rift (Rooney et al., 2005; Furman et al., 2006; Rooney et al., 2007; Rooney, 2010). Our Group 3 differs markedly from the Quaternary rift-floor volcanic in the MER by having much more enriched values of HREE and an overall flatter trace element profile. (d) Group 4a samples are plotted against contemporaneous Getra Kele rift margin basalts of southern Ethiopia (George and Rogers, 2002). While Group 4a plots with the Getra Kele basalts in terms of the more incompatible elements, there is a distinct heterogeneity between the two in terms of the more compatible elements – Group 4a samples are significantly more enriched. (e) Group 4b samples which likely are related to the Guguftu shield volcano are plotted against the two volcanic shields which have developed at this time (Guguftu and Choke; Kieffer et al., 2004). Group 4b overlaps with Guguftu basalts in terms of the more incompatible elements but display significant heterogeneity in terms of K, Th, and U. These variations may reflect lithospheric assimilation evident in the radiogenic isotope properties of these rocks.

dolerites were intruded during the period 20–12 Ma across the greater part of the margin. The timing coincides with the ~19–11 Ma syn-extensional Getra Kele basalts from southern Ethiopia (George and Rogers, 2002). In contrast, Group 4b dikes yield ages clustered around 24 Ma and are restricted to the Desse-Combolcha sector. These dikes are

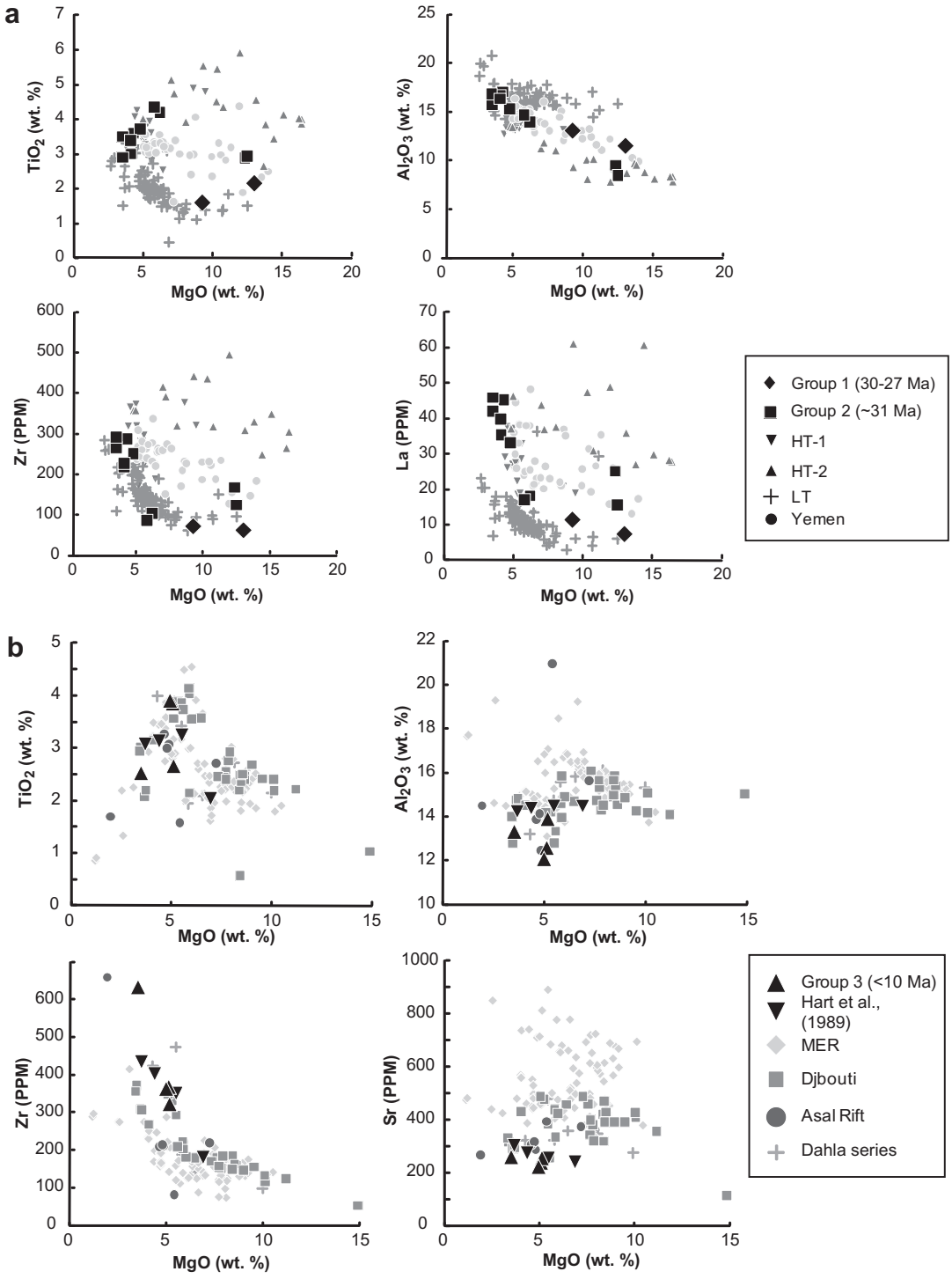

Fig. 4. MgO-X diagrams illustrating the variance between different Oligocene basalts in Ethiopia (Pik et al., 1999; Kieffer et al., 2004; Beccaluva et al., 2009) and Yemen (Baker et al., 1996b). (a) MgO-X diagrams illustrating the variance between our Group 3 and the 10 Ma-Recent activity in MER of Ethiopia (Rooney et al., 2005; Furman et al., 2006; Rooney et al., 2007; Rooney, 2010), Pliocene-Quaternary Djibouti, Quaternary Asal Rift, and 4–9 Ma Dahla series (Deniel et al., 1994). (b) MgO-X diagrams illustrating the variance between the rift margin and shield building phase of the Ethiopian plateau and Group 4 of this study. We show that Group 4a (19–12 Ma) is distinct from the contemporaneous Getra Kele formation of southern Ethiopia in most element plots (Stewart and Rogers, 1996; George and Rogers, 2002). The distinct major element trends (e.g. CaO/Al_2O_3) reflect the unusually deep clinopyroxene-dominated fractionation of the Getra Kele basalts (George and Rogers, 2002). Group 4b displays a similar range in trace elements when compared to the 22–25 Ma Choke and Guguftu shield volcanoes (Kieffer et al., 2004). Groups 4a can be distinguished easily from Group 4b, and displays elevated Zr.

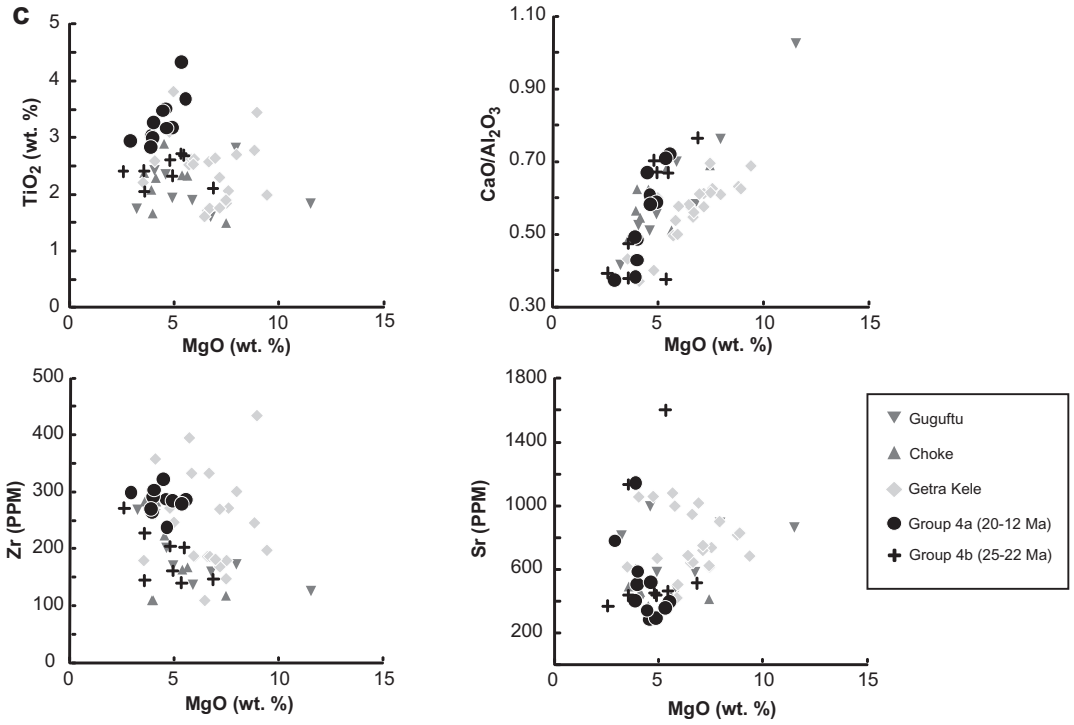

Fig. 4. (*continued*)

considered to be feeders for the earlier lavas of the ~22–25 Ma Guguftu shield volcano (Kieffer et al., 2004). Two isolated Group 4b dikes intruded east of Batie: mingled dolerite EKA-128, and evolved alkali trachyte EKA-134.

4.3. Isotope geochemistry

Twelve representative dolerites spanning the five chemical groups were selected for isotopic analysis (Table 4). The data plot within a three end-member mixing space defined by depleted mantle, Pan African lithosphere and the Afar plume mantle, as identified in studies of Quaternary basalts in Afar and the Ethiopian rift, and Gulf of Aden (Hart et al., 1989; Schilling et al., 1992; Deniel et al., 1994; Trua et al., 1999; Furman et al., 2006; Rooney et al., 2012a).

4.3.1. Groups 1 and 2 dikes

Group 1 have more radiogenic Pb isotopic compositions than the LT basaltic flows, and plot close to the "C" mantle reservoir (Hanan and Graham 1996; Fig. 5). However, other isotopic systems (Sr, Nd and Hf) are not consistent with a simple derivation from this single mantle reservoir (Figs. 6–8). In contrast, our single analyzed Group 2 sample, ankaramite sill EKA-112B, exhibits less radiogenic Pb isotopes that have elevated $^{207}Pb/^{204}Pb$ and $^{208}Pb/^{204}Pb$ at a given $^{206}Pb/^{204}Pb$ in comparison with HT-1 basalts from this region. These isotopic parameters do, however, plot consistently within the fields defined for Oligocene magmatism in Yemen (e.g., Baker et al., 1996a).

4.3.2. Group 3 dikes

Group 3 dolerites have the most radiogenic ε_{Hf} and ε_{Nd} (Fig. 7), and least radiogenic Sr (Fig. 6) and $^{207}Pb/^{204}Pb$ (Fig. 5) of all the samples analyzed in this study. The Pb isotope values overlap with those of the least radiogenic Quaternary Ethiopian rift basalts (Fig. 5), but Sr is significantly less radiogenic (Fig. 6) while Hf and Nd are more radiogenic (Fig. 7). These features link Group 3 dolerites to Djibouti and axial Gulf of Aden basalts. Western Afar margin basalts of similar age-range to the Group 3 dolerites, analyzed by previous authors (Hart et al., 1989), share common trace-element characteristics. However, these basalts exhibit less-radiogenic Pb isotopic signatures and typically form a broad trend, indicating the influence of the lithosphere on the erupted compositions (Fig. 5).

4.3.3. Group 4 dikes

Group 4 dolerites form an array in Pb-isotope space that indicates a substantial compositional heterogeneity between radiogenic and unradiogenic components (Fig. 5). The unradiogenic Pb component correlates with unradiogenic Nd and radiogenic Sr, interpreted here as Pan-African lithosphere. Group 4a dolerites overlap with, but do not extend to more radiogenic $^{206}Pb/^{204}Pb$ compositions (Fig. 5) displayed by the contemporaneous Getra Kele basalts in southern Ethiopia (Stewart and Rogers, 1996; George and Rogers, 2002). Indeed, substantial heterogeneity is evident between the two, where the radiogenic end-member of the Getra Kele Formation appears HIMU-like (George and Rogers, 2002), distinct from the "C" signature of the Afar plume present in all dike groups from the western Afar margin.

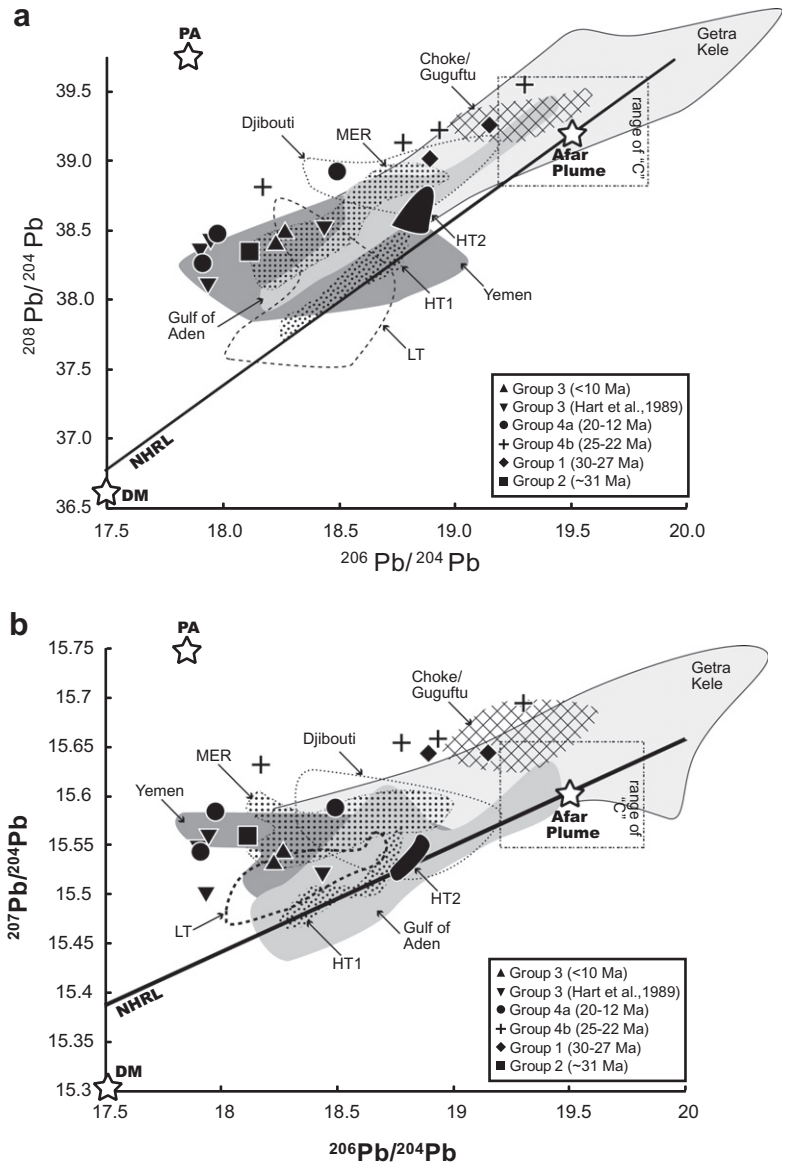

Fig. 5. Pb isotope variation plot showing our samples and other similar units in the region. (a) $^{208}Pb/^{204}Pb$ versus $^{206}Pb/^{204}Pb$. (b) $^{207}Pb/^{204}Pb$ versus $^{206}Pb/^{204}Pb$. Group 3 dikes are shown along with contemporaneous samples from western Afar reported by Hart et al. (1989). Data sources are: Getra Kele (Stewart and Rogers, 1996; George and Rogers, 2002); Choke/Guguftu (Kieffer et al., 2004); Djibouti includes Dahla, Asal rift and Pliocene-Quaternary basalts (Schilling et al., 1992; Deniel et al., 1994); MER-Main Ethiopian Rift (Furman et al., 2006; Rooney et al., 2012a); Gulf of Aden (Schilling et al., 1992); Yemen (Oligocene) (Baker et al., 1996b); western plateau HT1/HT2/LT (Pik et al., 1999; Kieffer et al., 2004). All data (our newly presented and existing data) older than ~10 Ma is age corrected. "C" is the mantle reservoir outlined by Hanan and Graham, 1996 and the assumed composition of the Afar Plume (Furman et al., 2006). Afar Plume, DM (depleted mantle) and PA (Pan African lithosphere) are endmembers modeled to contribute to magmatism in the region (Schilling et al., 1992; Rooney et al., 2012a). The northern hemisphere reference line (NHRL: Hart, 1984) is also drawn.

5. DISCUSSION

5.1. Revised chronostratigraphy for the Desse–Eloa traverse

The present study adds geochronological constraints to the existing stratigraphic record outlined for the western Afar margin at latitude 11°N (Table 1). We confirm that magmatic activity in the region commenced with voluminous fissure- and pipe-fed basalt eruptions ~31 Ma ago (Hofmann et al., 1997; Ukstins et al., 2002). The feeders for this pile comprise our Group 2 dolerites. Group 1 ankaramitic dikes are coincident with a period of major crustal extension and block faulting that followed the emplacement of the thick lava pile. Between 25 and 22 Ma, a period of localized magmatic activity is represented by closely spaced Group 4b dikes, feeders to the Guguftu Formation basalts

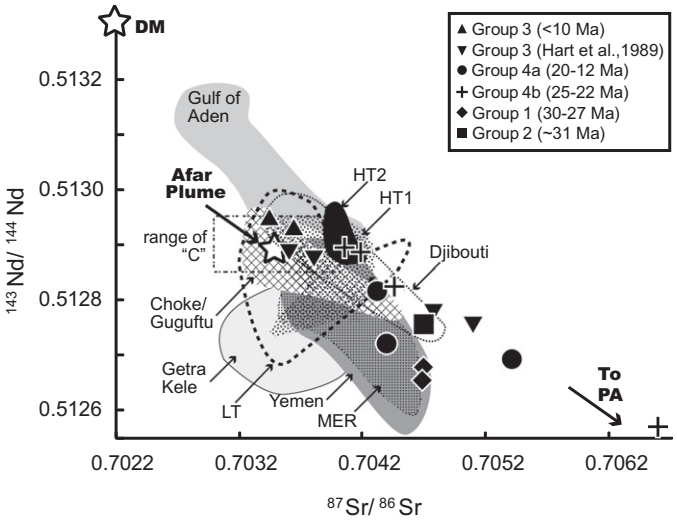

Fig. 6. $^{143}Nd/^{144}Nd$ vs $^{87}Sr/^{86}Sr$ variation for samples within this study and other similar units in the region. Endmembers and other regional datasets are those outlined in the caption of Fig. 5. Note that all isotopes are age corrected except those less than ~10 Ma. Group 1 overlaps the values for Yemen, plotting at more radiogenic Sr and unradiogenic Nd in comparison to most regional LT basalts, and consistent with an assimilation model. The single Group 2 dike plots near to the Yemen field. It is apparent that our Group 4b data broadly overlap Choke/Guguftu at the less radiogenic values of $^{87}Sr/^{86}Sr$ but fall at a slightly more radiogenic value for $^{143}Nd/^{144}Nd$. Group 4b extends towards extremely radiogenic $^{87}Sr/^{86}Sr$ values, typical of lithospheric contributions. Group 4a samples plot in a similar array but are displaced to lower values of $^{143}Nd/^{144}Nd$.

(Ukstins et al., 2002; Kieffer et al., 2004) which flowed from the plateau rim down into a small 'Stage 1' basin (Wolfenden et al., 2005).

Between 20 and 12 Ma, a third magmatic episode produced the Burka Formation basalts, ignimbrites and tuffs (Walter, 1980; Wolfenden et al., 2005) that accumulated in a 'Stage 2' basin immediately east of Batie. While the geochemistry of our Group 4a dikes matches that of the Burka formation basalts, these dikes occur over a wider region than Wolfenden et al.'s (2005) basin. The fourth and final magmatic episode within the Desse-Eloa transect produced the Upper Miocene Fursa basalts (Justin-Visentin and Zanettin, 1974). Renamed the Dahla Series by Wolfenden et al. (2005), they accumulated in a 'Stage 3' basin at the eastern end of the transect. Wolfenden et al. (2005) assign a period of 6.6–5.3 Ma to this series, but this activity may extend back to 10 Ma (Walter, 1980; Hart et al., 1989; Deniel et al., 1994). These lavas were fed by our Group 3 dikes which, however, are located in the central sector of the transect somewhat to the west of the 'Stage 3' basin.

5.2. Magmatic processes along the western Afar margin

The five magmatic groups defined along the western Afar margin are distinct in terms of REE patterns, and the origin of these patterns reflects magmatic processes active during the evolution of the Afar rift margin. To more effectively illustrate these distinctions we have undertaken a principal component analysis of the dolerite REE data. We have used a log-centered transform technique to overcome the constant sum constraint inherent to this form of statistical analysis (Aitchison, 1986).

$$Z_i = \mathrm{Log}(X_i / g(X_D)) \quad (1)$$

where: i = 1,...D, denoting elements of interest; Z_i is the log-centered transform for each element; X_i is the concentration of each element, i; $g(X_D)$ is the geometric mean of all elements of interest.

Approximately 96% of the variance is accounted for within the plane of the first two eigenvectors, and this increases to 97.8% with the addition of the third eigenvector. The first principal component (PC-1) is most influenced by the LREE and HREE, with less control from the MREE (Table 5), whereas the second principal component (PC-2) is dominantly influenced by LREEs and MREE (Fig. 9). The third principal component (PC-3) is dominated by

Table 5
Eigenvectors from our principal components analysis of the REE patterns in our Groups 1 to 4. For details of the analysis and interpretations refer to the text.

Element	PC1	PC2	PC3
La	0.27	−0.30	0.15
Ce	0.30	−0.18	0.21
Pr	0.31	−0.14	0.06
Nd	0.32	0.00	0.03
Sm	0.29	0.24	0.10
Eu	0.23	0.36	−0.75
Gd	0.15	0.53	−0.04
Tb	−0.08	0.56	0.55
Dy	−0.29	0.23	0.06
Ho	−0.32	0.05	0.02
Er	−0.32	−0.04	0.01
Yb	−0.31	−0.09	−0.17
Lu	−0.31	−0.12	−0.10

Eu, Tb and Ce and represents anomalous enrichments or depletions in these elements (e.g. plagioclase-related Eu anomaly) not accounted for by PC-1 and 2. To assess the root cause of these variations, we explore the various processes that may impact on the REE patterns.

To a first order, fractional crystallization of nominally anhydrous mafic gabbroic assemblages and assimilation of continental crust will elevate the LREE/HREE values in an evolving magma. PC-1 is sensitive to LREE and HREE variations and exhibits clear correlation with MgO, increasing sharply for Groups 2 and 3 at ~5% MgO (see Supplemental Data), though no clear correlation is evident for Groups 4a and 4b. These data may be interpreted to infer that below ~5% MgO, lithospheric assimilation and fractional crystallization processes control the REE behavior of these magmas. For this reason, interpretations of potential mantle processes are confined to dolerites with >5% MgO. This minimizes (but does not eliminate) the influence of gabbroic fractionation, lithospheric assimilation (Peate et al., 2008), and the complicating effects of REE-enriched phases that may become saturated in more evolved magmas (e.g. apatite and titanite: Bachmann and Bergantz, 2008).

Variability in the source and degree of melting are the dominant causes of REE heterogeneity in more primitive magmas. In a continental rifting environment, the lithospheric thickness determines the upper limit of the mantle melting column (Wang et al., 2002). Decreasing lithospheric thickness means a relative increase in melt from the shallower spinel lherzolite zone and relatively less melt from the deeper garnet lherzolite zone with a concomitant change in the MREE/HREE ratios of resulting magmas. Whilst lithospheric thinning may be an important ongoing process in southern and central Ethiopia (Rooney, 2010; Rooney et al., 2011), for the northern Ethiopian rift, located above the center of the ascending Oligocene plume head (Beccaluva et al., 2009), studies of temporal variation of lithospheric thickness have shown that substantial thinning must have occurred prior to or contemporaneous with the initial flood basalt event (Ayalew and Gibson, 2009).

In a plume-influenced environment, variable contributions from ambient upper mantle and the potentially diverse components hosted within the upwelling plume may have a significant impact on the trace element characteristics of resulting magmas. A temporal decrease in plume contribution (and a concomitant increase in role of the depleted upper mantle) should correspond to source depletion and a decrease in LREE/HREE (Schilling, 1973). On the other hand, the decrease in mantle potential temperature (T_P) when plume-influenced mantle is replaced with ambient upper mantle reduces the degree of melting and thus holds the LREE/MREE ratio relatively constant (Tegner et al., 1998; Hanghoj et al., 2003). Smaller contributions from a mantle plume to a melting column will result in a decreasing T_P, which will also impact the MREE/HREE ratios of generated magmas. A lower mantle T_P will initiate melting at shallower depths, thereby increasing the fraction of melt generated within the spinel lherzolite field, resulting in less fractionated MREE/HREE ratios. Further complexity arises when the role of pyroxenite in an upwelling plume is considered (Sobolev et al., 2005; Sobolev et al., 2007; Herzberg, 2011). The REE characteristics of these dikes are likely the result of multiple overlapping processes, and to resolve these we must establish the temporal heterogeneity in the contribution from the Afar plume to magmatism.

5.3. Temporal evolution of geochemical reservoirs along the western Afar margin

5.3.1. Geochemical reservoirs contributing to magmatism

Previous studies in the region have placed constraints as to the potential geochemical reservoirs contributing to magmatism in the Ethiopian magmatic province, typically by examining temporally restricted portions of the province (e.g., flood basalts or Quaternary rift activity: Pik et al., 1999; Rooney et al., 2012a). The suite of dikes that erupted along the western Afar margin is spatially restricted but temporally diverse, representing a 25 Myr window on the evolution of the magmatic reservoirs contributing to magmatism at a single location. The influence of a mantle plume is observed throughout the temporal magmatic record in East Africa (e.g., Rooney et al., 2012c). In modern magmas, the isotopic signature of a mantle plume is most pronounced towards Djibouti (Schilling et al., 1992; Rooney et al., 2012a), consistent with maximum T_P values recorded in this area (Rooney et al., 2012c). Another asthenospheric reservoir that displays characteristics that are broadly similar to the source of MORB is also necessary to fully account for the magmatic heterogeneity observed in Afar and along the Gulf of Aden (Schilling et al., 1992). The Pan-African lithosphere is a ubiquitous contributor to the magmatic heterogeneity observed in the region (Hart et al., 1989; Deniel et al., 1994; Trua et al., 1999; Furman et al., 2006). For the western Afar dikes, the contribution from Pan African lithospheric end-member increases with declining MgO, and can be interpreted as lithospheric (likely crustal) assimilation by asthenospheric melts during fractional crystallization in the crust. It is the interaction of these three reservoirs that accounts for the majority of geochemical heterogeneities observed in regional magmas.

Mixing models which were developed to account for the isotopic characteristics of Quaternary basalts from the Gulf of Aden and Main Ethiopian Rift have concluded that ternary mixing is evident between the Pan-African lithosphere, a depleted component thought to represent the upper mantle MORB source beneath the Gulf of Aden, and material derived from the Afar Plume (Schilling et al., 1992; Rooney et al., 2012a). These models further revealed complex patterns of reservoir interaction requiring the hybridization of the upper mantle MORB-like reservoir by mixing with foundered lithospheric materials (Rooney et al., 2012a). Using the same end-members and isotopic values, we have adopted the ternary mixing hypothesis of Rooney et al. (2012a) Table 6. To simplify the visualization of ternary mixing within the multi-isotope space (Sr-Nd-Pb-Hf) occupied by our samples, we have performed a principal component analysis (Fig. 10). The majority of isotopic variance is accounted for within the plane of the first two eigenvectors (97.1%), and therefore the isotopic variation is best illustrated by a PC-1/PC-2 projection. PC-1 is dominated by

heterogeneity in terms of the depleted upper mantle and Pan-African lithosphere end-members. While some variance on the PC-1 plane may be the result of a hybridized upper mantle (Rooney et al., 2012a), evidence of covariance of isotopic systems with MgO highlights the role of AFC processes for the western Afar dikes. PC-2 is most affected by contributions from the Afar plume end-member (Fig. 10).

5.3.2. Groups 1 and 2 dikes: flood basalt eruption and subsequent diking between 31 and 27 Ma

Our results indicate that the single isotopically characterized sample of HT-1 basalt (Group 2; EKA-112B) contains a significant contribution from depleted mantle and Pan-African lithosphere reservoirs. This observation is consistent with standard isotope plots showing EKA-112B falls closer to the Pan-African endmember in comparison to other regional HT-1 magmas. Group 1 dolerites, while having similar trace element characteristics to LT basalts of the western plateau, differ in that they carry little of the depleted mantle component that is ubiquitous in LT basalts elsewhere. Thus dolerite EKA-120 appears to have been derived from an almost binary mixture of Afar plume and pan-African lithosphere endmembers, and both Group 1 dolerites plot closer to the "C" reservoir than any previously analyzed flood basalt (Figs. 5 and 10). An important implication follows, that there is a decoupling between the isotopic and trace element characteristics of the Afar man-

Table 6
Endmember compositions used in plotting and for principal components analysis after Rooney et al. (2012a).

End member	ε_{Nd}	ε_{Hf}	$^{87}Sr/^{86}Sr$	$^{206}Pb/^{204}Pb$	$^{207}Pb/204Pb$	$^{208}Pb/^{204}Pb$
Pan African Lithosphere	−10.49	−15.35	0.7075	17.85	15.75	39.75
Depleted Mantle	13.89	22.24	0.7022	17.5	15.3	36.6
Afar Plume	4.62	9.27	0.7035	19.5	15.6	39.2

For Sr, Nd, and Pb the isotopic values for the depleted mantle and Pan African lithosphere endmembers are identical to Schilling et al. (1992). The Afar plume composition is set as the "C" mantle reservoir of Hanan and Graham (1996). To facilitate incorporating the Hf isotopic system into our interpretations, we make the assumption that the Afar plume and the regional upper mantle depleted end-members lie along the ε_{Nd}-ε_{Hf} mantle array ([1.4* ε_{Nd}]+2.8), thereby deriving ε_{Hf} from existing ε_{Nd} values (Table 6). The poorly constrained ε_{Hf} values for the Pan African lithosphere end-member likely lie below the mantle array, and to estimate them we performed a best-fit for Group 4b (this group extends to the least radiogenic values of ε_{Nd} and ε_{Hf}). We then derived ε_{Hf} from where this best-fit line intersects the plane defined by the modeled ε_{Nd} of the Pan African lithosphere end-member.

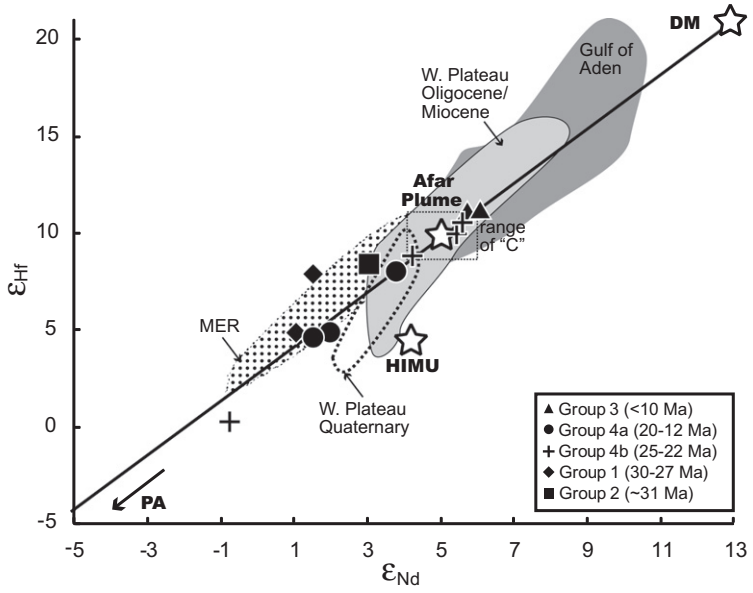

Fig. 7. Variation of samples from this study shown with a field outlining the only other data suites in the region that includes Hf isotopes. The undifferentiated Oligocene–Miocene western plateau basalts and Quaternary western plateau basalts presented by Meshesha et al. (2007; 2010) are shown here for reference. We also include Quaternary data from the Gulf of Aden and Main Ethiopian Rift (Rooney et al., 2012a). Trends shown in this plot broadly reflects other isotope systems – Groups 1 and 2 lie above the mantle array. In contrast Group 4b samples plot at or below the mantle array with increasing contributions from the Pan African endmember. This pattern is mirrored by the Miocene-Oligocene and Quaternary samples from the western plateau which extend to lower ε_{Hf} at the more differentiated end of the mixing array. While the precise value of ε_{Hf} for the PA endmember remains unclear, it is lower than the mantle array. Group 3 samples are more radiogenic than the "C" mantle reservoir, consistent with an increased role for the depleted mantle component in their genesis.

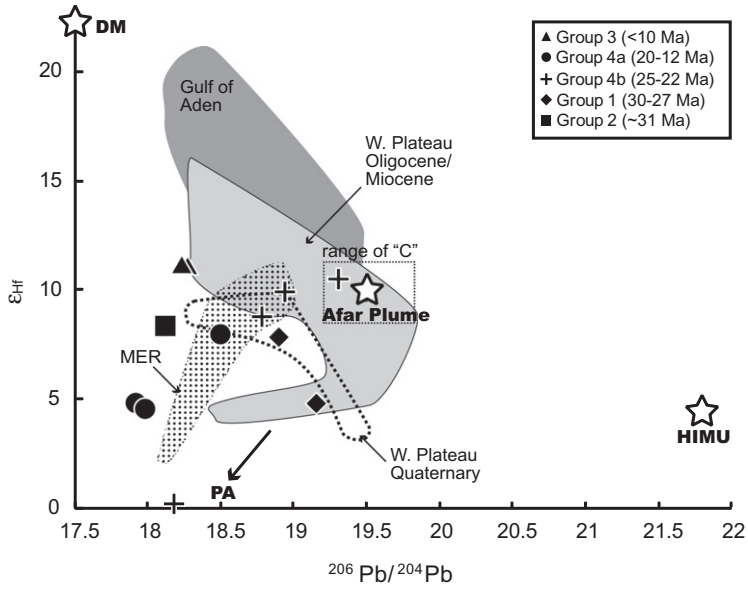

Fig. 8. ε_{Hf} shown against $^{206}Pb/^{204}Pb$ isotopes for samples from this study and other regional data suites (see Fig. 7 for data sources). This isotopic projection rules out a significant contribution from a HIMU-like reservoir in the petrogenesis of any of our samples. Furthermore, data from the undifferentiated Miocene-Oligocene western plateau rocks (which appear to extend towards HIMU in an ε_{Hf}-ε_{Nd} projection) are displaced towards unradiogenic Pb isotopes.

tle plume. Specifically, the isotopic characteristics of the radiogenic end-member of the Afar plume (e.g. radiogenic Pb isotopes), previously attributed only to the HT-2 basalts (Pik et al., 1999) can also be found in some LT basalts represented by our Group 1 dolerites.

5.3.3. Group 4 dikes: Shield volcanism between 25 and 12 Ma

Group 4b dolerites, which are related to the ~22–25 Ma Guguftu shield volcano, show evidence of mixing between the Afar plume and the pan African lithosphere components (Fig. 10). We suggest that plume-derived melts assimilated Pan-African crustal materials during magma differentiation. However, identity of the plume component in the ~25–22 Ma shield basalts is debated (Kieffer et al., 2004). Previous research notes that the Choke and Guguftu basaltic shield volcanoes have more elevated Pb isotopic values compared to the underlying Oligocene flood basalts (Kieffer et al., 2004). This isotopic heterogeneity is mirrored in the trace element characteristics, where the 25–22 Ma basalts bear similarities to Quaternary basalts in the Ethiopian rift and the northern Kenyan rift (Furman et al., 2004; Furman et al., 2006). The radiogenic end-member in the shield basalts of the western Ethiopian plateau has been interpreted to be a HIMU-like component within a complex upwelling (Kieffer et al., 2004), though the Pb isotopic values of these shield volcanoes lie close to the "C" mantle reservoir (Fig. 5). Hf isotopic data in this study preclude a dominantly HIMU-like component in the western Afar dikes, and instead favor derivation from a "C"-like reservoir (Figs. 7 and 8) similar to that for the Oligocene flood basalts (Marty et al., 1996; Furman et al., 2006).

From our data it is apparent that from ~30 to 22 Ma, the depleted mantle did not play a significant role in magma generation (Fig. 5), and as a result, the Pb isotope signature in basalts throughout this period reflects mixing between an endmember composed almost entirely of the Afar plume and the Pan African lithosphere. The modest degree of magmatism during this period (isolated shield volcanoes and dikes) argues against an increased plume flux in comparison to the initial flood basalt eruptions. However, potentially fertile and warm plume material located in the upper mantle that perhaps had not participated in melting during the initial flood basalt event or were part of a complex upwelling (Kieffer et al., 2004; Bastow et al., 2008; Rooney et al., 2012c) might be expected to melt preferentially as modest extension commenced along the Afar margin.

The 20–12 Ma interval represented by Group 4a dolerites in the Desse-Eloa transect correlates with a period of reduced basaltic volcanism around Afar, and coincided with ongoing lithospheric extension throughout the region. In addition to rifting along the western Afar margin, rifting at this time occurred in southern Ethiopia (Bonini et al., 2001), whilst sea-floor spreading was initiated in the Gulf of Aden and Red Sea (Bosworth et al., 2005, and references therein). The Group 4a dikes were therefore injected during an important dynamic phase in regional development of extension of the Afar margins. Group 4a dolerites plot close to the binary mixing region between Pan African lithosphere and the depleted mantle end-members (Figs. 5 and 10), implying a lesser contribution from the Afar plume, in sharp contrast to the 30–22 Ma time period (Fig. 5).

5.3.4. Group 3 dikes: evolution of rifting from 10 Ma to Recent

The period commencing at ~10 Ma marked the initiation of rifting in the northern Ethiopian rift and the eventual connection of the rift basins in Afar and central Ethiopia (Kazmin et al., 1981; Bonini et al., 2005; Wolfenden et al., 2005; Corti, 2009). Trace element and isotopic

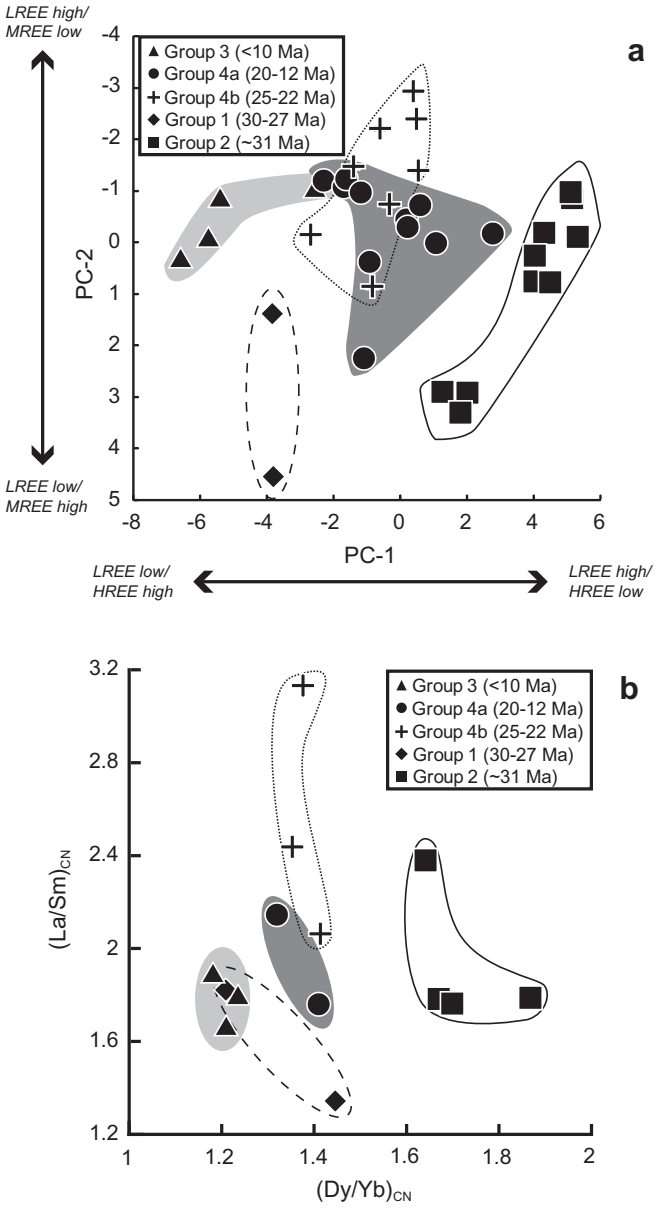

Fig. 9. (a) Score plot from our principal component analysis (PCA) of the REEs in our dike samples. See Table 5 for the details of PC1, 2 and 3. Dike groups are particularly apparent in this projection. See the main text and Table 5 for more details of the PCA analysis and description of the results. (b) REE ratio plot after Hanghoj et al. (2003). Samples approximately >5% MgO are shown here and values have been normalized to C1 chondrite. This projection illustrates the relative enrichment of LREE to MREE (La/Sm) and MREE to HREE (Dy/Yb).

characteristics of Group 3 dolerites indicate a more significant contribution from the depleted mantle in their petrogenesis in comparison to other groups (Figs. 2, 5, 7, 8 and 10). While this component is of the same magnitude as in Group 4a dolerites (e.g., EKA-106), the two are distinguished by smaller lithospheric contributions in the Group 3 dolerites (e.g., Fig. 10). Our data confirm previous studies on Afar margin lavas which show that, with decreasing age, the isotopic properties of the basalts express a more-depleted composition. This is interpreted simply as an increased contribution from the depleted upper mantle and a lessening of crustal assimilation (Hart et al., 1989). A similar pattern is observed in Djibouti where early volcanic products (>10 Ma) exhibit substantial lithospheric contributions, but which become insignificant as rifting and lithospheric thinning progress, replaced by an increasing fraction of melt derived from depleted upper mantle and the Afar plume (Deniel et al., 1994).

5.4. Rift evolution at the western Afar margin and comparisons to East Greenland

Tectonic thinning alone is an inadequate mechanism to explain the evolution of the East African Rift System (Ber-

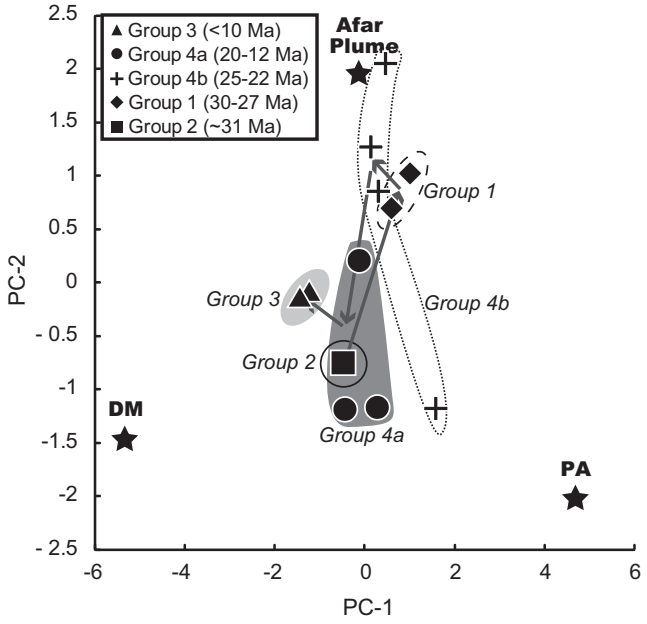

Fig. 10. Score plot from our PCA of the isotopic values for our dike Groups 1–4. This principal component analysis included ε_{Hf}, ε_{Nd}, and Sr in addition to the three Pb isotopes. Endmembers are: "C" – Afar plume, DM – depleted mantle, PA – Pan African lithosphere. The endmember values are listed in Table 6. PC-1 records the relative contributions from the DM and PA reservoirs while PC-2 reflects the contributions from the radiogenic "C" endmember interpreted as the Afar Plume. The general restriction of data to within the plane of these two eigenvectors is consistent with a ternary mixing model. The most radiogenic endmember of Group 4b may extend to outside of this mixing array, though heterogeneity in the plume endmember is likely. Samples from other studies (e.g. Hart et al., 1989) could not be plotted with this method as PCA requires each sample to have the same number of data values – no Hf data is available for most older datasets.

ckhemer et al., 1975; Mohr, 1983b). The concept that magmatic intrusions can significantly weaken the continental lithosphere, leading ultimately to its rupture, is now widely accepted in hypotheses of rift evolution (Klausen and Larsen, 2002; Buck, 2004; Buck, 2006; Bialas et al., 2010). The best exposed example of magma-rich breakup is the East Greenland continental margin, where glacier-cleared exposure reveals a regional pattern of diking, faulting and warping in a breakup zone initiated over a mantle plume (Myers, 1980; Klausen and Larsen, 2002; Hanghoj et al., 2003). The dikes along the western Afar margin share many of the same characteristics of the East Greenland dike swarm. The East Greenland swarm is broadly divided into an early stage of mafic diking that compositionally correlates with the regional flood basalt sequences, and a later less MgO-rich period of diking that does not correlate with the erupted flood basalts (Hanghoj et al., 2003). Similar to these observations, early dikes from western Afar are compositionally related to the regional flood basalt sequences and are relatively mafic. Later dikes from western Afar are similar to those from east Greenland that are typically less mafic and have no extrusive equivalent within the flood basalt sequence.

Statistical treatment of more than 1400 dikes (Klausen and Larsen, 2002) documents a progressive shift in orientation from predominantly subvertical inland to predominantly landward dipping (as low as 40°) offshore. This expresses the progressive seaward rotation of crustal units during the evolution of the margin (Morton and Black, 1975). Exposed dikes in the Afar margins are an order less numerous than in East Greenland. Nevertheless they share the same plateau-ward/inland dip, although an eastward decrease in the riftward dip angle of increasingly more abundant dikes is not observed along the Dessie-Eloa transect (cf. Wolfenden et al., 2005), perhaps a result of the cover of younger lavas in the easternmost part of the transect.

Our interpretation of the tectonic and magmatic evolution of the western Afar margin follows the three-stage rifting process proposed by Buck (2006): an initial stage of voluminous magmatic intrusion, an intermediate stage dominated by tectonic stretching, and a final stage where focused magmatic intrusion dominates strain accommodation:

5.4.1. Stage 1: voluminous magmatic intrusion

The initial stages of rifting coincide with the emplacement of melt at various levels within the lithosphere. Depending on the supply of magma, not all dikes may attain the surface. However, even small volumes of magma at the early stage of rift development may have a significant impact in subsequent rift evolution (Bialas et al., 2010). Within our study region the Group 2 dikes, related to the initial plume-head impact, strike rift-parallel precisely as predicted by models of initial magma-assisted rifting (Buck, 2006). The Ethiopian Oligocene flood-basalt pile attests to the enormous volumes of magma available to assist initiation of Afar margin rifting (Fig. 11A). The African lithosphere is considered to have a typical thickness of 120 km (Dugda et al., 2007), which requires some preliminary thinning process to have occurred before rifting could com-

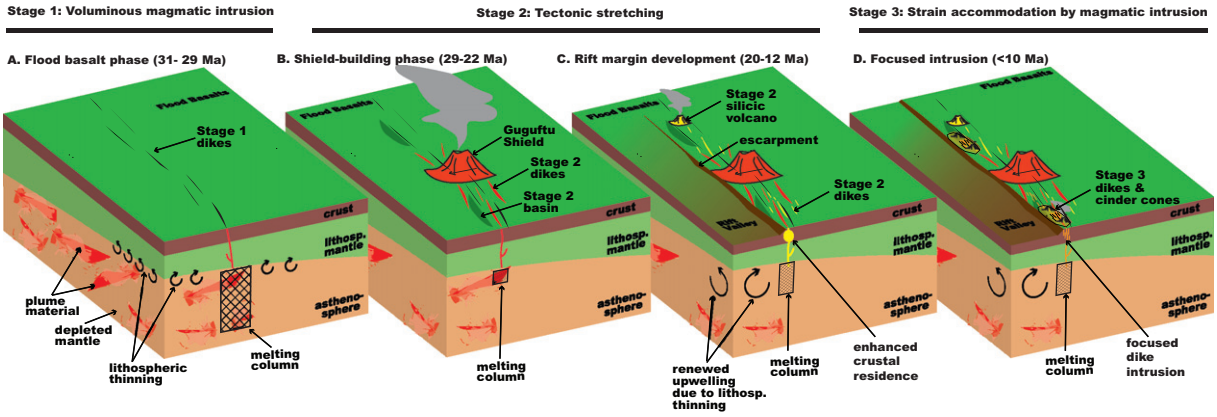

Fig. 11. Cartoon outlining a potential model for the evolution of the western Afar margin. These cartoons do not show contemporaneous activity within the rift (e.g., Rooney et al., 2011). See the text for a full narrative.

mence (Bialas et al., 2010). Existing studies (e.g., Ayalew and Gibson 2009), provide evidence that the necessary lithospheric thinning under Afar occurred during the impact of the Afar plume, perhaps from transformation and erosion at the base of the lithosphere, although the extent and magnitude of this thinning remain uncertain.

5.4.2. Stage 2: tectonic stretching

The second stage of rifting was characterized by a shift towards a greater degree of lithospheric stretching and faulting, proceeding rapidly in regions where previous magmatic injection had been voluminous (Bialas et al., 2010). Tectonic extension dominated this stage, while magmatism was greatly reduced. Whereas the initial, Oligocene flood-basalt event is well-represented in both Ethiopia and Yemen, the subsequent rifting of the African-Arabian continent involving the drift of Arabia away from the Afar plume reduced volcanic activity on the eastern flank of the Red Sea rift (Ukstins et al., 2002). In contrast, the western Afar margin preserves evidence of a wide temporal range of magmatic products, and offers insight into the relationship between magmatism and extension along an evolving rift margin. The diking associated with continued extension along the western Afar margin can be broadly divided on the basis of geochemistry into two events, represented by Group 4b dikes (Fig. 11B; 25–22 Ma), and Group 4a dikes (Fig. 11C; 20–12 Ma). They confirm that stretching and faulting of the western Afar crust was accompanied by local volcanism and magmatically induced subsidence that progressively moved riftwards with time (Fig 11C: Wolfenden et al., 2005).

Local diking and volcanism following the initial rifting of the Red Sea margin (Group 4b dikes; 25–22 Ma) was located at the rift border fault on the Desse-Eloa transect and fed construction of the Guguftu shield volcano on the plateau rim (Fig 11B: Kieffer et al., 2004; Wolfenden et al., 2005). Further riftward migration of strain was accompanied by local diking and volcanism (20–12 Ma), significantly closer to Afar (Fig 11C: Justin-Visentin and Zanettin, 1974; Morton et al., 1979). Nevertheless, a simple model of the younging of dikes towards the rift zone is complicated in the western Afar margin by overprinting. Contemporaneous lavas along the rift margin have a magmatic signature in common with the Desse-Eloa dolerites, revealing the assimilation of continental lithosphere by asthenosphere-derived basaltic magmas (e.g., Figs. 5 and 10), and the generation of a significant volume of silicic magmas (erupted as ignimbrites) derived by fractional crystallization of the same basalts (Ayalew and Gibson, 2009).

The increase in silicic volcanism during the 20–12 Ma period was related to the ongoing lithospheric extension. Fractional crystallization of basaltic magma rather than anatexis of continental crust was the major source for the silicic magmas of the Afar and rift valley margins (Ayalew et al., 2002; Peccerillo et al., 2003; Peccerillo et al., 2007; Ayalew and Gibson, 2009; Rooney et al., 2012b). A lessened magma supply rate, resulting in magmatic intrusion at greater depths and slower cooling (Behn et al., 2006), fostered crystal fractionation processes together with lithospheric assimilation. Additionally, rift faulting and fissuring within the continental crust facilitated shallow-level magmatic intrusion and differentiation (Antonellini and Cambray, 1992), together with stagnation of laterally migrating magma in the footwall of the faults (Bonini et al., 2001). Volcanic periodicity may reflect the complex relationship between magma chamber size, supply rate, and crystallinity (Jellinek and DePaolo, 2003). In rift margin environments, variations in the modeled strain field of a flexing plate (whereby melt at the base of the crust travels to the surface through fractures: Ellis and King, 1991) might also account for some degree of the periodicity of volcanism, allowing longer magma storage in the continental crust under the rift flanks. Accumulation of magma in the footwall of a rift border-fault can produce a feedback whereby rheology changes reduce the strength of the lithosphere, in turn resulting in a period of further faulting and intrusion (Bonini et al., 2001).

5.4.3. Stage 3: strain accommodation by magmatic intrusion

In the third and final stage of rift development, extension became focused at the rift axis (Mohr, 1978; Bilham et al., 1999; Ebinger and Casey, 2001; Casey et al., 2006; Rooney et al., 2011), manifested as intensive diking through severely thinned lithosphere (Ebinger and Casey, 2001;

Buck, 2004; Keranen et al., 2004; Wolfenden et al., 2005; Buck, 2006; Maguire et al., 2006). At this stage (<10 Ma), the western Afar margin was the site of local volcanism on a scale of segmentation similar to that of stage 2 but migrated closer to the rift floor (Fig. 11D). Group 3 dike samples have a significantly weaker lithospheric signature in comparison to Group 4a dikes, consistent with asthenospheric reservoirs becoming progressively more important in controlling the isotopic compositions of basaltic magmas as the rift margin evolved and magmatic injection became more focused (Hart et al., 1989; Deniel et al., 1994).

Our results show a temporal variation in the contribution of the Afar plume and depleted mantle to western Afar magmas, defined by an initial strong plume signature (Groups 1 and 4b) that becomes less pronounced in the later groups (Groups 3 and 4a; Fig. 10). Modest lithospheric thinning during the later development of the continental rift margin, from 20 Ma onward, facilitated decompressional melting of the depleted upper mantle (Figs. 5 and 10). Initially the western Afar margin at latitude 11°N was situated close to the center of the Afar plume during the flood-basalt event and initial rifting (Beccaluva et al., 2009), but continued lithospheric extension and the formation of new rift lithosphere then shifted the margin away from the plume center which is now located under Lake Abhe in central Afar (Schilling et al., 1992). The significant spatial heterogeneity among the late Cenozoic asthenospheric reservoirs contributing to magmatism beneath Djibouti and western Afar is surprising, considering the short distance (170 km) between the two regions (Schilling et al., 1992). It may reflect a progressively greater dispersion and preferential channeling of the Afar plume beneath the extending lithosphere (Sleep, 2008), which is consistent with geochemical, bathymetric, gravity, magnetic, and magneto-telluric data from the Gulf of Aden and Main Ethiopian Rift (Schilling et al., 1992; Leroy et al., 2010; Rooney et al., 2012a).

6. CONCLUSIONS

The western margin of Afar was formed by lithospheric and crustal extension accompanied by major diking and volcanism during the Oligocene to Quaternary evolution of the Afar rift basin. Magmatic activity, though varying in intensity throughout this evolution, spanned the entire history of the progressive continental rifting that formed the margin. Dike and lava samples from the margin now provide a window into the mantle sources and reservoirs involved, and the interaction and changing contributions from Afar plume, African lithosphere and depleted upper mantle melts. New $^{40}Ar/^{39}Ar$-geochronology places further constraints on the magmatic events of the margin, in which five broad episodes are revealed:

(1) The earliest dikes were contemporaneous with the 31–29 Ma flood-basalt province that covered much of Ethiopia and western Yemen (Fig. 11A). The geochemistry of these dikes resembles that of the HT-1 flood basalt flows which they intruded, though the dikes extend to significantly more mafic compositions (up to 12% MgO). The impact of the Afar mantle plume head at ~31 Ma initiated thinning of the overlying lithosphere and promoted melting of the depleted mantle and African lithosphere, generating magmas that were a broad mix of all three geochemical reservoirs.

(2) From ~30 to 27 Ma, a second, less intense stage of diking coincided with a broad lull in volcanic activity across the margin (Fig. 11B). The trace-element geochemistry of these dikes resembles that of the LT flood basalts, but isotopes reveal that the dike magmas contained a significantly elevated plume component compared with flood basalt magmas erupted elsewhere on the western Ethiopian plateau.

(3) From 25 to 22 Ma, formation of the Guguftu and Choke basaltic shields on the adjacent plateau coincided with a significant increase in margin diking (Fig. 11B). The basalts and dolerites share a similar geochemistry. The Afar plume contributed significantly to these magmas, although assimilation of African lithosphere (likely crust) supplied the heterogeneity evident in the radiogenic isotopic values. The minimal presence of a depleted mantle component from ~30 to 22 Ma could be the result of limited mantle upwelling due to the inferred small degree of lithosphere thinning during this time period.

(4) From 20 to 12 Ma, the evolving rift margin drifted away from the site of the plume. Decompressional melting of the depleted mantle became an important melt generation mechanism for the dike magmas as extension proceeded, though contributions from the Afar plume persisted. Widespread silicic magmatism across the margins of Afar was coincident with a spread of mafic diking (Fig. 11C) carrying a significant lithospheric component.

(5) The final stage of margin diking commenced at ~10 Ma. It coincided with the development of a spread of oblique faulting across the margin, and a narrow rift-parallel graben adjacent to the plateau (Fig. 11D). Magmatic intrusion was focused at two locations: at the easternmost sector of the margin, and in the marginal graben. Dikes and magmas of this period, like the preceding period, had a significant contribution from the depleted, asthenospheric mantle. However, further maturation of the margin led to a more established magmatic plumbing system at the riftward edge of the margin leading to a diminished lithospheric contribution to magmas of this period.

ACKNOWLEDGMENTS

The authors wish to thank Matthew Parsons, Chelsea Mack, Tim Matthews, Thomas Hudgins and Christian Briggs who assisted with sample preparation and analysis. Emmanuel Ponzevera performed the Neptune ICMPS measurements for Pb, Nd and Hf isotopes. PM expresses gratitude to Professor Pierre Gouin, S.J., for vital support at base during the original field mapping and sampling of the western Afar margin dikes in 1969. TR thanks Clifton Rooney for assistance with figures. Discussions with Dan McKenzie and Eric Grunsky assisted in our data interpretation. We thank

Wendy Nelson, Cindy Ebinger, Ian Bastow, and Derek Keir for comments that improved the manuscript. Ingrid Ukstins-Peate, Karen Hanghøj, and an anonymous reviewer provided detailed and helpful reviews which enhanced the manuscript. Finally we thank Steve Shirey for careful editorial handling.

APPENDIX A. SUPPLEMENTARY DATA

Supplementary data associated with this article can be found, in the online version, at http://dx.doi.org/10.1016/j.gca.2012.08.019.

REFERENCES

Abbate E., Azzaroli A., Zanettin B. and Visentin E. J. (1968) A geologic and petrographic mission of the "Consiglio Nazionale delle Ricerche" to Ethiopia 1967–1968 - Preliminary results. *Bollettino Società Geologica Italiana* **87**, 1–20.

Abbate E. and Sagri M. (1969) Datie considerazioni sul margine orientale dell'altopiano etiopico nell province del Tigrai e del Wollo. *Bollettino Società Geologica Italiana* **88**, 489–497.

Aitchison J. (1986) *The statistical analysis of compositional data*. Chapman and Hall, London, New York.

Antonellini M. A. and Cambray F. W. (1992) Relations between sill intrusions and dedding-parallel extensional shear zones in the Midcontinent Rift System of the Lake-Superior region. *Tectonophysics* **212**(3–4), 331–349.

Ayalew D., Barbey P., Marty B., Reisberg L., Yirgu G. and Pik R. (2002) Source, genesis, and timing of giant ignimbrite deposits associated with Ethiopian continental flood basalts. *Geochim. Cosmochim. Acta* **66**(8), 1429–1448.

Ayalew D. and Gibson S. A. (2009) Head-to-tail transition of the Afar mantle plume: Geochemical evidence from a Miocene bimodal basalt-rhyolite succession in the Ethiopian Large Igneous Province. *Lithos* **112**(3–4), 461–476.

Ayele A., Stuart G., Bastow I. and Keir D. (2007) The August 2002 earthquake sequence in north Afar: Insights into the neotectonics of the Danakil microplate. *J. Afr. Earth Sc.* **48**(2–3), 70–79.

Bachmann O. and Bergantz G. W. (2008) Rhyolites and their source mushes across tectonic settings. *J. Petrol.* **49**(12), 2277–2285.

Baker J., Snee L. and Menzies M. (1996a) A brief Oligocene period of flood volcanism in Yemen: Implications for the duration and rate of continental flood volcanism at the Afro-Arabian triple junction. *Earth Planet. Sci. Lett.* **138**(1–4), 39–55.

Baker J. A., Thirlwall M. F. and Menzies M. A. (1996b) Sr-Nd-Pb isotopic and trace element evidence for crustal contamination of plume-derived flood basalts: Oligocene flood volcanism in western Yemen. *Geochim. Cosmochim. Acta* **60**(14), 2559–2581.

Bastow I. D. and Keir D. (2011) The protracted development of the continent-ocean transition in Afar. *Nat. Geosci.* **4**(4), 248–250.

Bastow I. D., Nyblade A. A., Stuart G. W., Rooney T. O. and Benoit M. H. (2008) Rifting at the edge of the African low velocity anomaly. *Geochem. Geophys. Geosyst.* **Q12022**. http://dx.doi.org/10.1029/2008GC002107.

Bastow, I.D., Pilidou, S., Kendall, J.M. and Stuart, G.W., 2010. Melt-Induced seismic anisotropy and magma assisted rifting in Ethiopia: evidence from surface waves. Geochemistry Geophysics Geosystems: Q0AB05, doi:10.1029/2010GC003036.

Beccaluva L., Bianchini G., Natali C. and Siena F. (2009) Continental flood basalts and mantle plumes: a case study of the Northern Ethiopian Plateau. *J. Petrol.* **50**(7), 1377–1403.

Behn M. D., Buck W. R. and Sacks I. S. (2006) Topographic controls on dike injection in volcanic rift zones. *Earth Planet. Sci. Lett.* **246**(3–4), 188–196.

Berckhemer H., Baier B., Bartelsen H., Behle A., Burkhardt H., Gebrande H., Makris J., Menzel H., Miller H. and Vees R. (1975) Deep seismic soundings in the Afar region and on the highland of Ethiopia. In *Afar between continental and oceanic rifting* (eds. A. Pilger and A. Roesler). Schweizerbart, Stuttgart, pp. 89–107.

Bialas R. W., Buck W. R. and Qin R. (2010) How much magma is required to rift a continent? *Earth Planet. Sci. Lett.* **292**, 68–78.

Bilham R., Bendick R., Larson K., Mohr P., Braun J., Tesfaye S. and Asfaw L. (1999) Secular and tidal strain across the main Ethiopian rift. *Geophys. Res. Lett.* **26**(18), 2789–2792.

Bonini, M., Corti, G., Innocenti, F., Manetti, P., Mazzarini, F., Abebe, T. and Pecskay, Z., 2005. Evolution of the Main Ethiopian Rift in the frame of Afar and Kenya rifts propagation. Tectonics, 24(1): TC1007, doi: 10.1029/2004TC00168.

Bonini M., Sokoutis D., Mulugeta G., Boccaletti M., Corti G., Innocenti F., Manetti P. and Mazzarini F. (2001) Dynamics of magma emplacement in centrifuge models of continental extension with implications for flank volcanism. *Tectonics* **20**(6), 1053–1065.

Bosworth W., Huchon P. and McClay K. (2005) The Red Sea and Gulf of Aden basins. *J. Afr. Earth Sc.* **43**(1–3), 334–378.

Boynton W. V. (1984) Cosmochemistry of the rare earth elements: meteorite studies. In *Rare earth element geochemistry* (ed. P. Henderson). Elsevier, New York.

Buck W. R. (2004) Consequences of asthenospheric variability on continental rifting. In *Rheology and deformation of the lithosphere at continental margins* (eds. G. Karner, B. Taylor, N. W. Driscoll and D. L. Kohlstedt). Columbia University Press, New York, pp. 1–30.

Buck W. R. (2006) The role of magma in the development of the Afro-Arabian rift system. In *The Afar Volcanic Province within the East African Rift System* (eds. G. Yirgu, C. Ebinger and P. Maguire). Special Publication of the Geological Society, London, pp. 43–54.

Casey M., Ebinger C., Keir D., Gloaguen R. and Mohamed F. (2006) Strain accomodation in transitional rifts: Extension by magma intrusion and faulting in Ethiopian rift magmatic segments. In *The Afar Volcanic Province within the East African Rift System* (eds. G. Yirgu, C. Ebinger and P. Maguire). Geological Society, London, pp. 143–164.

Catanzaro E. J., Murphy T. J., Shields W. R. and Garner E. L. (1968) Absolute isotopic abundance ratios of common equal-atom and radiogenic lead isotopic standards. *Journal of Research of the National Bureau of Standards: Section a-Physics and Chemistry* **72A**(3), 26.

Corti G. (2009) Continental rift evolution: From rift initiation to incipient break-up in the Main Ethiopian Rift. *East Africa. Earth-Science Reviews* **96**(1–2), 1–53.

Daly E., Keir D., Ebinger C. J., Stuart G. W., Bastow I. D. and Ayele A. (2008) Crustal tomographic imaging of a transitional continental rift: the Ethiopian rift. *Geophys. J. Int.* **172**(3), 1033–1048.

Deering C. D., Cole J. W. and Vogel T. A. (2008) A rhyolite compositional continuum governed by lower crustal source conditions in the Taupo Volcanic Zone. *New Zealand. Journal of Petrology* **49**(12), 2245–2276.

Deniel C., Vidal P., Coulon C. and Vellutini P. J. (1994) Temporal evolution of mantle sources during continental rifting - the volcanism of Djibouti (Afar). *Journal of Geophysical Research-Solid, Earth* **99**(B2), 2853–2869.

Dugda, M.T., Nyblade, A.A. and Julia, J., 2007. Thin lithosphere beneath the Ethiopian plateau revealed by a joint inversion of

Rayleigh wave group velocities and receiver functions. Journal of Geophysical Research-Solid, Earth, 112(B8): B08305, doi:10.1029/2006JB004918.

Ebinger C., Ayele A., Keir D., Rowland J., Yirgu G., Wright T., Belachew M. and Hamling I. (2010) Length and Timescales of Rift Faulting and Magma Intrusion: The Afar Rifting Cycle from 2005 to Present. *Annu. Rev. Earth Planet. Sci.* **38**(38), 439–466.

Ebinger C. J. and Casey M. (2001) Continental breakup in magmatic provinces: An Ethiopian example. *Geology* **29**(6), 527–530.

Ebinger C. J. and Sleep N. H. (1998) Cenozoic magmatism throughout East Africa resulting from impact of a single plume. *Nature* **395**(6704), 788–791.

Ellis M. and King G. (1991) Structural control of flank volcanism in continental rifts. *Science* **254**(5033), 839–842.

Fialko Y. A. and Rubin A. M. (1999) Thermal and mechanical aspects of magma emplacement in giant dike swarms. *J. Geophys. Res.* **104**(B10), 23033–23049.

Frey H. M., Lange R. A., Hall C. M., Delgado-Granados H. and Carmichael I. S. E. (2007) A Pliocene ignimbrite flare-up along the Tepic-Zacoalco rift: Evidence for the initial stages of rifting between the Jalisco block (Mexico) and North America. *Geol. Soc. Am. Bull.* **119**(1–2), 49–64.

Furman T., Bryce J. G., Karson J. and Iotti A. (2004) East African Rift System (EARS) plume structure: Insights from quaternary mafic lavas of Turkana. *Kenya. Journal of Petrology* **45**(5), 1069–1088.

Furman T., Bryce J. G., Rooney T., Hanan B. B., Yirgu G. and Ayalew D. (2006) Heads and tails: 30 million years of the Afar plume. In *The Afar Volcanic Province within the East African Rift System* (eds. G. Yirgu, C. Ebinger and P. Maguire). Special Publication of the Geological Society, London, pp. 95–120.

George R. M. and Rogers N. W. (2002) Plume dynamics beneath the African Plate inferred from the geochemistry of the Tertiary basalts of southern Ethiopia. *Contrib. Miner. Petrol.* **144**(3), 286–304.

Gortani M. and Bianchi A. (1937) Osservazioni geologiche e petrografiche nella regione di Harar (Africa Orientale Italiana). *Bollettino Società Geologica Italiana* **56**, 499–516.

Gortani M. and Bianchi A. (1973) *Itinerari geologici nella Dancalia meridionale e sugli altipiani Hararini Missione Geologica dell'AGIP nella Dancalia Meridionale e sugli Altipiani Hararini (1936–1938)*. Accademia Nazionale Lincei, Roma, 240.

Hall C. M. and Farrell J. W. (1995) Laser Ar-40/Ar-39 ages of tephra from Indian-Ocean deep-sea sediments - tie points for the astronomical and geomagnetic polarity Time Scales. *Earth Planet. Sci. Lett.* **133**(3–4), 327–338.

Hanan B. B. and Graham D. W. (1996) Lead and helium isotope evidence from oceanic basalts for a common deep source of mantle plumes. *Science* **272**(5264), 991–995.

Hanghoj K., Storey M. and Stecher O. (2003) An isotope and trace element study of the East Greenland Tertiary dyke swarm: Constraints on temporal and spatial evolution during continental rifting. *J. Petrol.* **44**(11), 2081–2112.

Hart S. R. (1984) A large-scale isotope anomaly in the southern-hemisphere mantle. *Nature* **309**(5971), 753–757.

Hart W. K., Woldegabriel G., Walter R. C. and Mertzman S. A. (1989) Basaltic volcanism in Ethiopia - Constraints on continental rifting and mantle interactions. *Journal of Geophysical Research-Solid Earth and Planets* **94**(B6), 7731–7748.

Herzberg C. (2011) Identification of Source Lithology in the Hawaiian and Canary Islands: Implications for Origins. *J. Petrol.* **52**(1), 113–146.

Hofmann C., Courtillot V., Feraud G., Rouchett P., Yirgu G., Ketefo E. and Pik R. (1997) Timing of the Ethiopian flood basalt event and implications for plume birth and global change. *Nature* **389**(6653), 838–841.

Huismans R. S., Podladchikov Y. Y. and Cloetingh S. (2001) Transition from passive to active rifting: Relative importance of asthenospheric doming and passive extension of the lithosphere. *Journal of Geophysical Research-Solid, Earth* **106**(B6), 11271–11291.

Hyodo H. and York D. (1993) The discovery and significance of a fossilized radiogenic argon wave (Argonami) in the Earth's crust. *Geophys. Res. Lett.* **20**(1), 61–64.

Jellinek A. M. and DePaolo D. J. (2003) A model for the origin of large silicic magma chambers: precursors of caldera-forming eruptions. *Bull. Volcanol.* **65**(5), 363–381.

Jepsen, D.H. and Athearn, M.J., 1962. East-west geologic sections, Blue Nile river basin, Ethiopia. Dept. of Water Resources, Addis Ababa, Drawing No. 5.2 BN-3.

Justin-Visentin E. and Zanettin B. (1974) Dike swarms, volcanism and tectonics of the Western Afar margin along the Kombolcha-Eloa traverse (Ethiopia). *Bull. Volcanol.* **38**, 187–205.

Kazmin V., Berhe S. M. and Wondm-Agennehu B. (1981) *Geological map of the Ethiopian Rift*. The Ethiopian Government - Ministry of Mines, Energy and Water Resources, Addis Ababa.

Keir, D., Belachew, M., Ebinger, C.J., Kendall, J.M., Hammond, J.O.S., Stuart, G.W., Ayele, A. and Rowland, J.V., 2011a. Mapping the evolving strain field during continental breakup from crustal anisotropy in the Afar Depression. Nature, Communications, 2.

Keir D., Hamling I. J., Ayele A., Calais E., Ebinger C., Wright T. J., Jacques E., Mohamed K., Hammond J. O. S., Belachew M., Baker E., Rowland J. V., Lewi E. and Bennati L. (2009) Evidence for focused magmatic accretion at segment centers from lateral dike injections captured beneath the Red Sea rift in Afar. *Geology* **37**(1), 59–62.

Keir, D., Pagli, C., Bastow, I.D. and Ayele, A., 2011b. The magma-assisted removal of Arabia in Afar: Evidence from dike injection in the Ethiopian rift captured using InSAR and seismicity. Tectonics, 30.

Keranen K., Klemperer S. L., Gloaguen R., Asfaw L., Ayele A., Ebinger C., Furman T., Harder S., Keller G. R., Mackenzie G. D., Maguire P. K. H. and Stuart G. W. (2004) Three-dimensional seismic imaging of a protoridge axis in the main Ethiopian Rift. *Geology* **32**(11), 949–952.

Kieffer B., Arndt N., Lapierre H., Bastien F., Bosch D., Pecher A., Yirgu G., Ayalew D., Weis D., Jerram D. A., Keller F. and Meugniot C. (2004) Flood and shield basalts from Ethiopia: Magmas from the African superswell. *J. Petrol.* **45**(4), 793–834.

Klausen M. and Larsen H. (2002) East Greenland coast-parallel dike swarm and its role in continental breakup. In *Volcanic Rifted Margins* (eds. M. Menzies, S. L. Klemper, C. J. Ebinger and J. Baker). Geological Society of America, Boulder, Co., pp. 133–158.

Leroy S., d'Acremont E., Tiberi C., Basuyau C., Autin J., Lucazeau F. and Sloan H. (2010) Recent off-axis volcanism in the eastern Gulf of Aden: Implications for plume-ridge interaction. *Earth Planet. Sci. Lett.* **293**, 140–153.

Maguire P., Keller G. R., Klemper S. L., Mackenzie G., Keranen K., Harder S., O'Reilly B., Thybo H., Asfaw L., Kahn M. and Amha M. (2006) Crustal structure of the Northern Main Ethiopian Rift from the EAGLE controlled source survey; a snapshot of incipient lithospheric break-up. In *The Afar Volcanic Province within the East African Rift System* (eds. G. Yirgu, C. Ebinger and P. Maguire). Special Publication of the Geological Society, London, pp. 269–292.

Manhes G., Minster J. F. and Allegre C. J. (1978) Comparative uranium-thorium-lead and rubidium-strontium study of Saint-

Severin amphoterite - consequences for early Solar-System chronology. *Earth Planet. Sci. Lett.* **39**(1), 14–24.

Marty B., Pik R. and Gezahegn Y. (1996) Helium isotopic variations in Ethiopian plume lavas; nature of magmatic sources and limit on lower mantle contribution. *Earth Planet. Sci. Lett.* **144**(1–2), 223–237.

Megrue G. H., Norton E. and Strangway D. W. (1972) Tectonic history of Ethiopian Rift as deduced by K-Ar ages and paleomagnetic measurements of basaltic dikes. *J. Geophys. Res.* **77**(29), 5744–5754.

Meshesha D. and Shinjo R. (2007) Crustal contamination and diversity of magma sources in the northwestern Ethiopian volcanic province. *J. Mineral. Petrol. Sci.* **102**, 272–290.

Meshesha D. and Shinjo R. (2010) Hafnium isotope variations in Bure volcanic rocks from the northwestern Ethiopian volcanic province. a new insight for mantle source diversity. *J. Mineral. Petrol. Sci.* **105**, 101–111.

Mohr P. (1971) *Ethiopian Tertiary dike swarms, 339*. Smithsonian Institution, Research in Space Science, SAO Special Report, 339.

Mohr P. (1978) Afar. *Annu. Rev. Earth Planet. Sci.* **6**, 145–172.

Mohr P. (1983a) Ethiopian flood basalt province. *Nature* **303**(5918), 577–584.

Mohr P. (1983b) The Morton-Black hypothesis for the thinning of continental-crust revisited in western Afar. *Tectonophysics* **94**(1–4), 509–528.

Mohr P. (1999) The Asmara dike swarm, Eritrean Plateau; physical parameters of an off-rift olivine dolerite injection zone. *Acta Vulcanol.* **11**(1), 177–181.

Mohr P. A. (1962) The Ethiopian rift system. *Bulletin of the Geophysical Observatory* **3**(1), 33–62.

Morton W. H. and Black R. (1975) Crustal attenuation in Afar. In *Afar Depression of Ethiopia* (eds. A. Pilger and A. Rosler). Schweizerbart, Stuttgart, pp. 55–65.

Morton W. H., Rex D. C., Mitchell J. G. and Mohr P. (1979) Riftward younging of volcanic units in the Addis Ababa region. *Ethiopian Rift valley. Nature* **280**(5720), 284–288.

Myers J. S. (1980) Structure of the coastal dyke swarm and associated plutonic intrusions of East Greenland. *Earth Planet. Sci. Lett.* **46**(3), 407–418.

Peate D. W., Barker A. K., Riishuus M. S. and Andreasen R. (2008) Temporal variations in crustal assimilation of magma suites in the East Greenland flood basalt province. Tracking the evolution of magmatic plumbing systems. *Lithos* **102**(1–2), 179–197.

Peccerillo A., Barberio M. R., Yirgu G., Ayalew D., Barbieri M. and Wu T. W. (2003) Relationships between mafic and peralkaline silicic magmatism in continental rift settings: A petrological, geochemical and isotopic study of the Gedemsa volcano, central Ethiopian rift. *J. Petrol.* **44**(11), 2003–2032.

Peccerillo A., Donati C., Santo A. P., Orlando A., Yirgu G. and Ayalew D. (2007) Petrogenesis of silicic peralkaline rocks in the Ethiopian rift: Geochemical evidence and volcanological implications. *J. Afr. Earth Sc.* **48**(2–3), 161–173.

Pik R., Deniel C., Coulon C., Yirgu G., Hofmann C. and Ayalew D. (1998) The northwestern Ethiopian Plateau flood basalts. Classification and spatial distribution of magma types. *J. Volcanol. Geoth. Res.* **81**(1–2), 91–111.

Pik R., Deniel C., Coulon C., Yirgu G. and Marty B. (1999) Isotopic and trace element signatures of Ethiopian flood basalts; evidence for plume-lithosphere interactions. *Geochim. Cosmochim. Acta* **63**(15), 2263–2279.

Renne P. R., Deckart K., Ernesto M., Féraud G. and Piccirillo E. M. (1996) Age of the Ponta Grossa dike swarm (Brazil), and implications to Paranáflood volcanism. *Earth Planet. Sci. Lett.* **144**(1–2), 199–211.

Rooney, T., Furman, T., Bastow, I.D., Ayalew, D. and Gezahegn, Y., 2007. Lithospheric modification during crustal extension in the Main Ethiopian Rift. Journal of Geophysical Research, B, Solid Earth and Planets, 112: B10201, doi:10.1029/2006JB004916.

Rooney T., Furman T., Yirgu G. and Ayalew D. (2005) Structure of the Ethiopian lithosphere: Xenolith evidence in the Main Ethiopian Rift. *Geochim. Cosmochim. Acta* **69**(15), 3889–3910.

Rooney T. O. (2010) Geochemical evidence of lithospheric thinning in the southern Main Ethiopian Rift. *Lithos* **117**(1–4), 33–48.

Rooney T. O., Bastow I. D. and Keir D. (2011) Insights into extensional processes during magma assisted rifting: evidence from aligned scoria cones and maars. *J. Volcanol. Geoth. Res.* **201**(1–4), 83–96.

Rooney T. O., Hanan B. B., Graham D. W., Furman T., Blichert-Toft J. and Schilling J.-G. (2012a) Upper Mantle Pollution during Afar Plume–Continental Rift Interaction. *J. Petrol.* **53**, 365–389.

Rooney T. O., Hart W. K., Hall C. M., Ayalew D., Ghiorso M. S., Hidalgo P. and Yirgu G. (2012b) Peralkaline magma evolution and the tephra record in the Ethiopian Rift. *Contrib. Miner. Petrol.*. http://dx.doi.org/10.1007/s00410-012-0744-6.

Rooney T. O., Herzberg C. and Bastow I. D. (2012c) Elevated mantle temperature beneath East Africa. *Geology* **40**(1), 27–30.

Samson S. D. and Alexander E. C. (1987) Calibration of the interlaboratory Ar-40 Ar-39 dating standard, Mmhb-1. *Chem. Geol.* **66**(1–2), 27–34.

Schilling J. G. (1973) Afar Mantle Plume - rare-earth evidence. *Nature-Physical Science* **242**(114), 2–5.

Schilling J. G., Kingsley R. H., Hanan B. B. and McCully B. L. (1992) Nd-Sr-Pb isotopic variations along the Gulf of Aden - Evidence for Afar mantle plume continental lithosphere interaction. *Journal of Geophysical Research-Solid, Earth* **97**(B7), 10927–10966.

Schultz R. A., Soliva R., Fossen H., Okubo C. H. and Reeves D. M. (2008) Dependence of displacement-length scaling relations for fractures and deformation bands on the volumetric changes across them. *J. Struct. Geol.* **30**(11), 1405–1411.

Sleep N. H. (2008) Channeling at the base of the lithosphere during the lateral flow of plume material beneath flow line hot spots. *Geochem. Geophys. Geosyst.* **9**, Q08005. http://dx.doi.org/10.1029/2008GC002090.

Sobolev A. V., Hofmann A. W., Kuzmin D. V., Yaxley G. M., Arndt N. T., Chung S. L., Danyushevsky L. V., Elliott T., Frey F. A., Garcia M. O., Gurenko A. A., Kamenetsky V. S., Kerr A. C., Krivolutskaya N. A., Matvienkov V. V., Nikogosian I. K., Rocholl A., Sigurdsson I. A., Sushchevskaya N. M. and Teklay M. (2007) The amount of recycled crust in sources of mantle-derived melts. *Science* **316**(5823), 412–417.

Sobolev A. V., Hofmann A. W., Sobolev S. V. and Nikogosian I. K. (2005) An olivine-free mantle source of Hawaiian shield basalts. *Nature* **434**(7033), 590–597.

Stewart K. and Rogers N. (1996) Mantle plume and lithosphere contributions to basalts from southern Ethiopia. *Earth Planet. Sci. Lett.* **139**(1–2), 195–211.

Sun S. s. and McDonough W. F. (1989) Chemical and isotopic systematics of oceanic basalts: Implications for mantle composition and processes. In *Magmatism in the ocean basins* (ed. A. D. Saunders). Geological Society, London, pp. 313–345.

Tanaka T., Togashi S., Kamioka H., Amakawa H., Kagami H., Hamamoto T., Yuhara M., Orihashi Y., Yoneda S., Shimizu H., Kunimaru T., Takahashi K., Yanagi T., Nakano T., Fujimaki H., Shinjo R., Asahara Y., Tanimizu M. and Dragusanu C. (2000) JNdi-1: a neodymium isotopic reference in consistency with LaJolla neodymium. *Chem. Geol.* **168**(3–4), 279–281.

Tegner C., Lesher C. E., Larsen L. M. and Watt W. S. (1998) Evidence from the rare-earth-element record of mantle melting for cooling of the tertiary Iceland plume. *Nature* **395**(6702), 591–594.

Tilton G. R. (1973) Isotopic lead ages of chondritic meteorites. *Earth Planet. Sci. Lett.* **19**(3), 321–329.

Trua T., Deniel C. and Mazzuoli R. (1999) Crustal control in the genesis of Plio-Quaternary bimodal magmatism of the Main Ethiopian Rift (MER); geochemical and isotopic (Sr, Nd, Pb) evidence. *Chem. Geol.* **155**(3–4), 201–231.

Turner, G. and Cadogan, P.H., 1974. Possible effects of 39Ar recoil in 40Ar dating., Proceedings of the Fifth Lunar Science Conference, 1601–1615.

Turner, G., Enright, M.C. and Cadogan, P.H., 1978. The early history of chondrite parent bodies inferred from 40Ar-39Ar ages, Proceedings of the Lunar and Planetary Science Conference, 989–1025.

Ukstins I. A., Renne P. R., Wolfenden E., Baker J., Ayalew D. and Menzies M. (2002) Matching conjugate volcanic rifted margins; 40Ar/39Ar chrono-stratigraphy of pre- and syn-rift bimodal flood volcanism in Ethiopia and Yemen. *Earth Planet. Sci. Lett.* **198**(3–4), 289–306.

van Wijk J., van Hunen J. and Goes S. (2008) Small-scale convection during continental rifting: Evidence from the Rio Grande rift. *Geology* **36**(7), 575–578.

Vogel T. A., Flood T. P., Patino L. C., Wilmot M. S., Maximo R. P. R., Arpa C. B., Arcilla C. A. and Stimac J. A. (2006) Geochemistry of silicic magmas in the Macolod Corridor, SW Luzon, Philippines: evidence of distinct, mantle-derived, crustal sources for silicic magmas. *Contrib. Miner. Petrol.* **151**(3), 267–281.

Walker G. P. L. (1960) Zeolite zones and dike distribution in relation to the structure of the basalts of Eastern Iceland. *Journal of Geology* **68**(5), 515–528.

Walter R. C. (1980) *The volcanic history of the Hadar early-man site and the surrounding Afar region of Ethiopia*. Case Western Reserve University, Ph.D., 426 pp.

Wang, K., Plank, T., Walker, J.D. and Smith, E.I., 2002. A mantle melting profile across the basin and range, SW USA. Journal of Geophysical Research-Solid, Earth, 107(B1): 2017, doi:10.1029/2001JB0002092.

White R. and McKenzie D. (1989) Magmatism at rift zones - the generation of volcanic continental margins and flood basalts. *Journal of Geophysical Research-Solid Earth and Planets* **94**(B6), 7685–7729.

Wolfenden E., Ebinger C., Yirgu G., Renne P. R. and Kelley S. P. (2005) Evolution of a volcanic rifted margin: Southern Red Sea. *Ethiopia. Geological Society of America Bulletin* **117**(7–8), 846–864.

Wright, T.J., Sigmundsson, C.P., C., Belachew, M., Hamling, I., Brandsdottir, B., Keir, D., Pedersen, R., Ayele, A., Ebinger, C., Einarsson, P., Lewi, E. and Calais, E., 2012. Geophysical constraints on the dynamics of spreading centres from 1 rifting episodes on land. Nature Geoscience, In Press.

Zanettin B. (1992) Evolution of the Ethiopian Volcanic Province. *Memorie Lincee Scienze Fisiche e Naturali* **1**, 155–181.

Associate editor: Steven B. Shirey